

ABSTRACT

Title of thesis: BACKSTEPPING CONTROL DESIGN
 FOR THE COORDINATED MOTION OF
 VEHICLES IN A FLOWFIELD

Rochelle Mellish, Master of Science, 2011

Thesis directed by: Dr. Derek A. Paley
 Department of Aerospace Engineering

Motion coordination of autonomous vehicles has applications from target surveillance to climate monitoring. Previous research has yielded stabilizing formation control laws for a self-propelled vehicle model with first-order rotational dynamics; however this model does not adequately describe the rotational and translational dynamics of vehicles in the atmosphere or ocean. This thesis describes the design of decentralized algorithms to control self-propelled vehicles with second-order rotational and translational dynamics. Backstepping controls for parallel and circular formations are designed in the absence of a flowfield and in a steady, uniform flowfield. Backstepping and proportional-integral controllers are then used to stabilize yaw in a rigid-body model. Feedback linearization is used to attain the desired forward speed. These formation control laws extend prior results to a more realistic vehicle model. Aside from the addition of new sensing and communication requirements, the second-order control laws are demonstrated to have comparable performance to the first-order controllers. The theoretical results are illustrated by numerical simulations.

BACKSTEPPING CONTROL DESIGN FOR THE
COORDINATED
MOTION OF VEHICLES IN A FLOWFIELD

by

Rochelle Mellish

Thesis submitted to the Faculty of the Graduate School of the
University of Maryland, College Park in partial fulfillment
of the requirements for the degree of
Master of Science
2011

Advisory Committee:
Dr. Derek A. Paley, Chair/Advisor
Professor Balakumar Balachandran
Dr. J. Sean Humbert

© Copyright by
Rochelle Mellish
2011

Acknowledgments

My deepest gratitude goes to my Lord and Savior Jesus Christ – from whom all blessings flow. This experience has truly been a blessing, because I have had the opportunity to contribute to the field of aerospace engineering. From early on, it has been evident to me that it is God who directed my steps to be here.

I'd like to thank my advisor, Dr. Paley, for giving me an invaluable opportunity to work on challenging and interesting projects during my time at Maryland. It has been a pleasure to work with and learn from him.

My gratitude also goes to the other graduate students in the Collective Dynamics and Control Laboratory, whose company has brightened my days at Maryland.

Looking back to my initial days at the University of Maryland, I extend special thanks to Dr. Pines for believing in my ability to succeed in graduate school. I would also like to acknowledge Ms. Rosalia Webb for her assistance and advice, which truly brightened my first year here.

I owe the sincerest thanks to my parents. They have stood by my side in everything that I have wanted to do. They have prayed without ceasing for me, and devoted much of their time to my well-being.

Lastly, I would like to acknowledge financial support for the work of this thesis from the Office of Naval Research (ONR), and I would like to thank the Alfred P. Sloan Foundation Graduate Scholarship Program and the University of Maryland Department of Aerospace Engineering for their financial support of my graduate studies.

Rochelle Mellish

Dedication

This thesis is dedicated to my family.

Table of Contents

List of Figures	v
List of Symbols	vii
1 Introduction	1
1.1 First-Order Rotational Dynamics and the Particle Model	7
1.2 Rigid Motions in $SE(2)$	10
1.3 Review of Parallel and Circular Formations	12
2 Backstepping Control Design	16
2.1 Overview	16
2.2 Backstepping and the Particle Model	19
3 Control of Second-Order Rotational Dynamics via Backstepping	22
3.1 Parallel Formation Control	22
3.2 Circular Formation Control	26
4 Control of Second-Order Rotational Dynamics in a Uniform Flowfield	31
4.1 Parallel Formation Control	31
4.2 Circular Formation Control	34
5 Considerations for Implementing the Backstepping Control	38
5.1 Computing the Steering Control for Vehicles in a Flowfield	38
5.2 Sensing and Communication Requirements	39
5.3 Comparison to Proportional Control	40
6 Extension to Planar Rigid-Body Dynamics	43
7 Control of Planar Rigid-Body Dynamics	49
7.1 Parallel Formation Control	49
7.2 Circular Formation Control	52
8 Control of Planar Rigid-Body Dynamics in a Uniform Flowfield	60
8.1 Parallel Formation Control	62
8.2 Circular Formation Control	67
9 Conclusion	72
A Appendix: Alternate Drag Model	74
Bibliography	81

List of Figures

1.1	Autonomous vehicles [7, 31, 23]	3
1.2	First-order vehicle model: particles with similar movement capabilities to nonholonomic carts.	7
1.3	(a) A single particle in the plane. (b) A single particle in a flowfield.	8
1.4	Block diagram for the first-order particle model.	11
1.5	Block diagram for the first-order particle model in terms of shape variables.	15
3.1	Block diagram for the second-order vehicle model.	23
3.2	(a) Synchronized motion of self-propelled vehicles with second-order rotational dynamics. The dotted-line trajectories indicate that a parallel formation has been attained. (b) Turning rate of each vehicle, stabilized to zero using the backstepping-based controller. The vehicles have been randomly initialized.	26
3.3	(a) Stabilization of a circular formation of self-propelled vehicles with second-order rotational dynamics. (b) The steady-state turning rate of each vehicle is $\omega_0 = 1$. The vehicles have been randomly initialized.	29
4.1	(a) Stabilization of a parallel formation in a uniform, time-invariant flowfield $\alpha = 0.5$. (b) Turning rate of each vehicle, stabilized to zero using the backstepping-based controller. Randomly-generated initial conditions.	34
4.2	(a) Stabilization of a circular formation in a uniform, time-invariant flowfield $\alpha = 0.5$. (b) The steady-state turning rate of each vehicle is $\omega_0 = 1$ (shown for only one vehicle). Randomly-generated initial conditions.	37
5.1	Block diagram for the second-order vehicle model in terms of shape variables.	40
6.1	(a) Rigid-body model (b) Reference frames, no flow (c) Reference frames in flowfield f	46
6.2	Block diagram for the rigid-body model.	48
7.1	(a) Rigid-body parallel motion in the plane. (b) Velocity component of parallel motion. Randomly-generated initial conditions.	50
7.2	Illustration of the condition $\dot{U}_{par} = 0$. p is the initialization point in \mathbb{R}^6	52
7.3	(a) Rigid-body circular motion in the plane. (b) Velocity component of circular motion with time. Randomly-generated initial conditions.	54
7.4	Illustration of the condition $\dot{U}_{circ} = 0$. p is the initialization point in \mathbb{R}^6	56

8.1	(a) Rigid body parallel motion in a flowfield. Blue arrows represent the direction of heading; red arrows represent the total velocity. (b) Crab angles β_k and $\hat{\beta}_k$ with time. Randomly initialized.	64
8.2	Illustration of the condition $\dot{U}_{par} = 0$ in a flowfield. p is the initialization point in \mathbb{R}^6	66
8.3	Diagram of the modified vehicle, with a moment couple realized by control surfaces at the tail and nose.	67
8.4	Circular motion in a flowfield (a) without a prescribed center and (b) with a prescribed center at $[0, 0]$. Black arrows show the direction of heading, red arrows indicate the total velocity. Randomly-generated initial conditions.	69
8.5	(a) Locally-measured crab angle.(b) Inertially-measured crab angle with time. Results are shown for only one vehicle.	70
8.6	(a) Total speed s_k in the body frame. (b) Inertially-measured speed of the k th vehicle. Results are shown for only one vehicle.	71
8.7	Steady-state error $\omega_0 \hat{s}_k - \dot{\hat{\beta}}_k - \omega_k$ vs. time. Results are shown for all vehicles.	71
A.1	A rigid-body in a uniform flowfield. The drag is assumed to act a distance l_1 from the center of mass.	74

List of Symbols

r_k	position of k th vehicle
θ_k	velocity heading of k th vehicle
u_k	steering control for first-order vehicle representation
a_k	steering control for second-order vehicle representation
λ_k	steering control for second-order vehicle representation in flowfield
$\eta_{1,k}$	real coordinate of vehicle velocity (backstepping)
$\eta_{2,k}$	imaginary coordinate of vehicle velocity (backstepping)
$\eta_{3,k}$	representation of k th vehicle's velocity heading (backstepping)
$\tau_{1,k}$	real coordinate of vehicle velocity in flowfield
$\tau_{2,k}$	imaginary coordinate of vehicle velocity in flowfield
$\tau_{3,k}$	representation of k th vehicle's velocity heading in flowfield
ξ_k	k th vehicle's turning rate (backstepping)
ω_k	k th vehicle's turning rate (rigid-body)
Ω_k	k th vehicle's turning rate when a flowfield is present (backstepping)
f_k	flowfield as measured by the k th vehicle
α	magnitude of real flow component
γ_k	inertial velocity heading of the k th vehicle (particle model)
s_k	total speed of the k th vehicle
\hat{s}_k	inertial speed of the k th vehicle in rigid body model
ω_0	curvature of circular trajectory
c_k	center of the k th vehicle's circular trajectory
ϕ_k	desired first-order rotational dynamics
P	$N \times N$ projector matrix
u_k	forward velocity in the k th body frame
v_k	sideslip velocity in the k th body frame
ρ	fluid density
S	vehicle reference area
C_D	drag coefficient
D_k	drag of k th vehicle
T_k	thrust of k th vehicle
F_k	steering force of k th vehicle
l	distance from vehicle center of mass to steering force application
m_0	mass of vehicle
I_0	moment of inertia of vehicle
β_k	crab angle of k th vehicle
$\hat{\beta}_k$	inertially-measured crab angle of k th vehicle
ψ_k	$\theta_k + \beta_k$
γ_k	$\theta_k + \hat{\beta}_k$ (inertial velocity heading, rigid-body model)

Chapter 1

Introduction

Research in motion coordination of autonomous vehicles is directly applicable to a number of defense and environmental scenarios, including surveillance [11, 21], wind and temperature measurement for climate monitoring [35], and modeling of the collective behavior of biological systems [30]. In many applications of coordinated motion, each vehicle in the network is not controlled by a central computer, but rather by a computer on each vehicle. Each agent communicates with its neighbors to automatically control its relative position and orientation [8]. This decentralized communication and control framework enables each group member to act independently and makes the group robust to the failure of an individual agent [20].

Ongoing research in the coordinated motion of autonomous vehicles has focused on the stabilization of planar formations of self-propelled particles. In prior work, each particle controls the rate of change of the orientation of its velocity; hence, the rotational dynamics are first-order differential equations [33]. The steering control is modeled as a force orthogonal to the particle's velocity so that the particle's direction of travel is under control, but the speed is constant [24]. Formation control laws for this particle model have been developed for parallel and circular formations in the absence of a flowfield [33] and in a uniform, time-invariant flowfield [27]. All-to-all and limited communication frameworks have been considered

[33, 34].

Expressing the controllers in terms of *shape variables* rather than group variables reduces sensing requirements and is possible when the global location of the group is not related to the goal configuration [36]. For instance, the control laws used to drive the particle models presented in [33] are referred to as *shape control* laws because the variables that appear in the controllers may be expressed in terms of relative positions and relative orientations between pairs of particles [15].

In the model of steering control introduced here, the steering control regulates the angular acceleration of the velocity orientation. This level of control is particularly relevant in the context of planar rigid-body motion, where a dynamic vehicle model must account not only for motion of the agent's center of mass, but also for rotational motion about the center of mass. This second-order model is used to derive a control law that stabilizes the velocity orientation of each particle relative to the other particles in a formation. The control design follows the iterative process of integrator backstepping, in which the existing states of the first-order model are recursively used to stabilize steady motions of the second-order model [1, 32].

Recent work in the control of multi-agent systems has incorporated the backstepping control design technique [14]. In [6] backstepping is used to design a controller that will regulate the second-order translational dynamics in order to stabilize a planar formation of three vehicles. The communication framework is modeled as a directed graph, and the goal configuration is a triangular formation. The goal of this thesis is different than [6] in that parallel and circular formations of self-propelled particles are considered. These two motion primitives can be achieved by

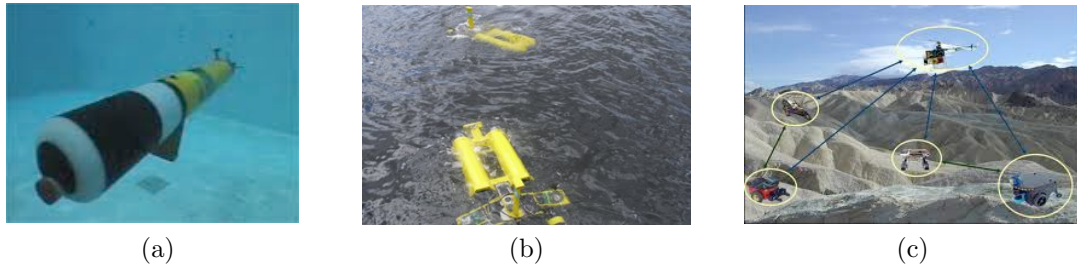


Figure 1.1: Autonomous vehicles [7, 31, 23]

an unlimited number of vehicles, and they serve as the basis for more complicated collective patterns [33].

The addition of second-order rotational dynamics is a step in the way of adapting the particle model to a network of physical platforms; however, the backstepping control laws are implemented on platforms modeled as unicycles, so that they can only move forward and turn. There are generally two control inputs in such models: a speed controller and a steering controller. In general, sometimes the capabilities of the platform are constrained further, as is the case when the turning rate of the platform is saturated or the speed of the platform is constant. Examples of constant-speed vehicle models that rely solely on steering control are described in [33, 15, 27, 34, 5, 24].

Implementing cooperative control laws based on particle dynamics enables the location of the vehicle's center of mass to be controlled. Additional control inputs must be considered to ensure that not only the desired angular orientation is achieved, but also that the forward and sideslip speeds converge to the desired values. Although there are numerous dynamic models that focus on the development of motion-planning algorithms for mobile robots, most consider only a single platform

rather than a group. One example is [10], in which the motion-planning output of a kinematic model is used with a dynamic rigid-body model in order to develop a trajectory for an autonomous vehicle. Another example is [9], in which a Lagrangian formulation is used to derive the dynamic equations of a single mobile robot with non-holonomic constraints. To regulate movement of the robot, a velocity controller is used to generate torque control by way of integrator backstepping.

There is also a sizeable body of work that focuses on producing kinematic motion models for each agent in a group, however, many such models typically do not incorporate rigid-body dynamics. An example of a kinematic control for a multi-agent system is [18], in which integrator backstepping is used for formation control of multiple non-holonomic agents.

A similar approach has been used in the present work, in which a vehicle model based on [33] and [27] with second-order rotational dynamics is introduced. Using the previously-mentioned backstepping controllers to generate yaw commands, a collection of planar rigid bodies with second-order translational and rotational dynamics is considered. This rigid-body model rotates and translates with a variable speed that results in thrust, steering, and drag forces. By extending existing steering control laws via backstepping and providing a new speed control, the planar rigid-body model achieves comparable closed-loop performance to particle models, even in the presence of a flowfield.

This work most closely resembles that of [3], in which motion planning for multiple marine surface vehicles was studied. The authors implemented a yaw controller and a line-of-sight guidance law. A coordinate transform was used to ease

the control design, because the yaw controller appeared in the transverse dynamics. In regard to formation control, their primary focus was on formations similar to the parallel formation considered in this thesis, although in addition to heading, they also controlled the inter-vehicle separation distances. In the related paper [4], motion planning for multiple surface vehicles was studied when ocean currents were present. However, only non-curved desired trajectories were treated. In the present work, it is shown that with the original vehicle dynamics in a parallel formation, the crab angle converges to zero. Furthermore, in the present work the case of circular formations in a flowfield are also treated; in this scenario, the transverse dynamics do not converge to zero, but rather vary with the heading.

Another closely-related work is [13], which provides an example of decentralized thrust and steering coordinated path-following of multiple underactuated rigid bodies, with the goal being to achieve consensus. The vehicle model used in this publication is very similar to the one introduced in the present work. However, the control design is extremely sensitive to initial conditions, whereas the controllers designed in the current work are robust to the choice of initial conditions.

The contribution of this thesis is to present steering and thrust control algorithms for the stabilization of parallel and circular formations in a rigid-body model. Using integrator backstepping, stabilizing steering controls are provided in the absence of a flowfield and then in the presence of a moderate-strength, time-invariant flowfield. In the latter case, the flowfield is assumed to be known, uniform, and steady. The backstepping control laws retain the shape-control characteristics of their first-order counterparts, where the shape space includes the derivative of the

relative orientations. The results of the first-order model are preserved under the second-order rotational dynamics, as long as each vehicle knows its own turning rate. The solutions of the closed-loop system are illustrated with simulations. Using the steering controllers developed via backstepping, decentralized thrust and steering controllers are then provided for a collection of identical planar rigid bodies in a uniform flowfield. These controllers enable the swarm to achieve parallel and circular formations. Feedback linearization is used to design the thrust controller, and both backstepping and proportional-integral controls are used to design the steering controller. Idealized hydrodynamic effects on the vehicle are modeled, summarized as a drag term. The rigid-body dynamics are stabilized so that each platform moves with constant speed (relative to the flow) in the desired formation.

The outline of this thesis is as follows. In the remainder of the current chapter, the particle model, the parallel formation control law, and the circular formation controller are introduced. In Chapter 2, a brief summary is provided of backstepping control design while relating it to the particle model with and without a flowfield. In Chapter 3, a backstepping controller is presented for the flow-free model. In Chapter 4, the backstepping design is repeated for motion coordination in a uniform, time-invariant flowfield. Chapter 5 discusses considerations that should be made when implementing the proposed controllers on an autonomous vehicle and compares the backstepping controller to a proportional controller. Chapter 6 reviews an existing second-order vehicle model and describes the rotational and translational dynamics of a set of idealized planar rigid bodies. Chapter 7 derives the controllers used to stabilize parallel and circular formations of the rigid body model when no flowfield is

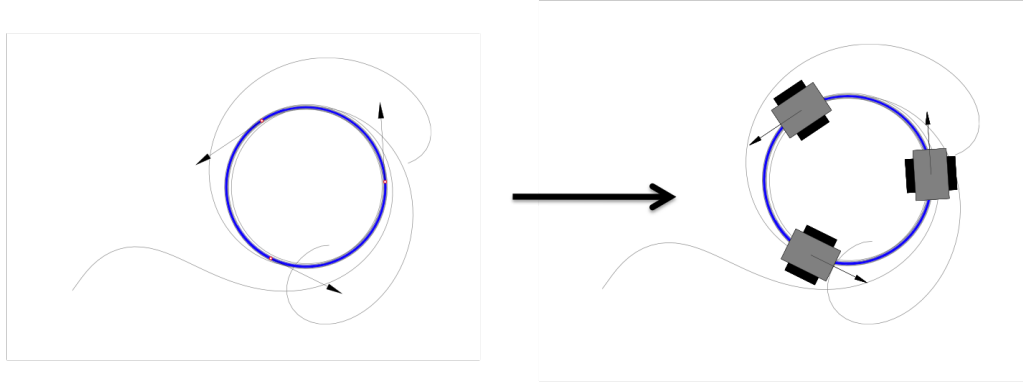


Figure 1.2: First-order vehicle model: particles with similar movement capabilities to nonholonomic carts.

present. Chapter 8 illustrates the stabilization of parallel and circular formations in a known, uniform flowfield. Chapter 9 summarizes the thesis and ongoing research.

1.1 First-Order Rotational Dynamics and the Particle Model

To design a backstepping control for planar collective motion, we begin by defining the particle model for particle motion in the absence of a flowfield [33]. Let r_k be the position of the k th particle and $\dot{r}_k = e^{i\theta_k}$ be its (unit) velocity. We have

$$\begin{aligned}\dot{r}_k &= e^{i\theta_k} \\ \dot{\theta}_k &= u_k,\end{aligned}\tag{1.1}$$

where $k = 1, \dots, N$ and u_k represents the steering control. We rewrite these equations in real coordinates so that the original states and control now represent the

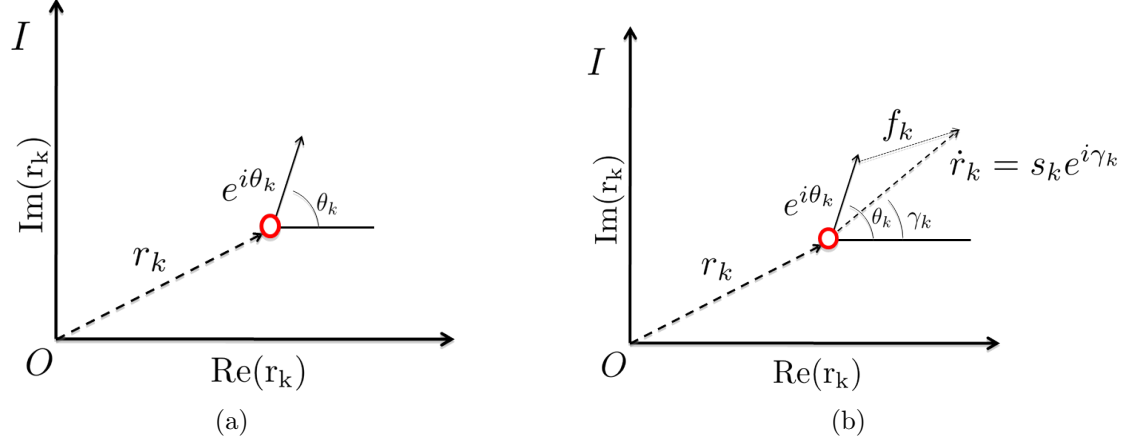


Figure 1.3: (a) A single particle in the plane. (b) A single particle in a flowfield.

first component of a higher-ordered system; that is,

$$\begin{aligned}
 \dot{\eta}_{1,k} &= \cos \eta_{3,k} \\
 \dot{\eta}_{2,k} &= \sin \eta_{3,k} \\
 \dot{\eta}_{3,k} &= \xi_k.
 \end{aligned} \tag{1.2}$$

$\eta_{1,k}$, $\eta_{2,k}$, and $\eta_{3,k}$ represent the state variables $\text{Re}\{r_k\}$, $\text{Im}\{r_k\}$, and θ_k , respectively. $\xi_k = u_k$ is the state-feedback control, which is expressed in terms of the shape variables $\theta_j - \theta_k$ and $(r_k - r_j)e^{i\theta_k}$. Shape variables are further discussed later in this chapter and in Chapter 5. The higher-ordered system with control a_k of the rotational acceleration $\dot{\xi}_k = \ddot{\theta}_k$ is

$$\begin{aligned}
 \dot{\eta}_{1,k} &= \cos \eta_{3,k} \\
 \dot{\eta}_{2,k} &= \sin \eta_{3,k} \\
 \dot{\eta}_{3,k} &= \xi_k \\
 \dot{\xi}_k &= a_k,
 \end{aligned} \tag{1.3}$$

where a_k is the control input that we design using backstepping. Similar to the first-order case, this higher-level controller is expressed in terms of shape variables; we introduce a new shape variable, $\xi_j - \xi_k$, to represent the angular rate of vehicle j with respect to k .

When an external flowfield is considered, the particle model (1.1) becomes [27]

$$\begin{aligned}\dot{r}_k &= e^{i\theta_k} + f_k \\ \dot{\theta}_k &= u_k.\end{aligned}\tag{1.4}$$

The flowfield measured at the location of the k th particle is given by f_k , where $f_k \in \mathbb{C}$. The model (1.4) can be rewritten as [27]

$$\begin{aligned}\dot{r}_k &= s_k e^{i\gamma_k} \\ \dot{\gamma}_k &= w_k.\end{aligned}\tag{1.5}$$

The variables $s_k = |e^{i\theta_k} + f_k|$ and $\gamma_k = \arg\{e^{i\theta_k} + f_k\}$ represent the magnitude and orientation of the particle's inertial velocity, respectively, and w_k is the control. For a uniform, time-invariant flow f_k oriented along the real axis, $f_k = \alpha$, where $\alpha < 1$. In this case, s_k becomes [27]

$$s_k = \alpha \cos \gamma_k + \sqrt{1 - \alpha^2 \sin^2(\gamma_k)} > 0.\tag{1.6}$$

With the addition of a flowfield f_k , the model (1.3) becomes¹

$$\begin{aligned}
 \dot{\eta}_{1,k} &= \cos \eta_{3,k} + \langle f_k, 1 \rangle \\
 \dot{\eta}_{2,k} &= \sin \eta_{3,k} + \langle f_k, i \rangle \\
 \dot{\eta}_{3,k} &= \xi_k \\
 \dot{\xi}_k &= a_k.
 \end{aligned} \tag{1.7}$$

Similar to the expression we used for (1.5), we may express (1.7) in terms of the particle speed, s_k . We use the variable $\tau_{3,k}$ to represent the orientation of the k th particle's *inertial* velocity. The control of the higher-ordered system is represented by λ_k , rather than by the variable a_k of the flow-free model (1.3). Thus, the entire higher-ordered system with uniform, time-invariant flow becomes

$$\begin{aligned}
 \dot{\tau}_{1,k} &= s_k \cos \tau_{3,k} \\
 \dot{\tau}_{2,k} &= s_k \sin \tau_{3,k} \\
 \dot{\tau}_{3,k} &= \Omega_k \\
 \dot{\Omega}_k &= \lambda_k,
 \end{aligned} \tag{1.8}$$

where λ_k is the control of the rotational acceleration $\dot{\Omega}_k = \ddot{\gamma}_k$.

1.2 Rigid Motions in $SE(2)$

The state of each vehicle at any time t can be expressed in terms of the vehicle's position, attitude, translational velocity, and angular velocity. The rotation of the

¹We use the inner product $\langle x, y \rangle = \text{Re}\{\bar{x}y\}$, where $x, y \in \mathbb{C}$. \bar{x} is the complex conjugate of x .

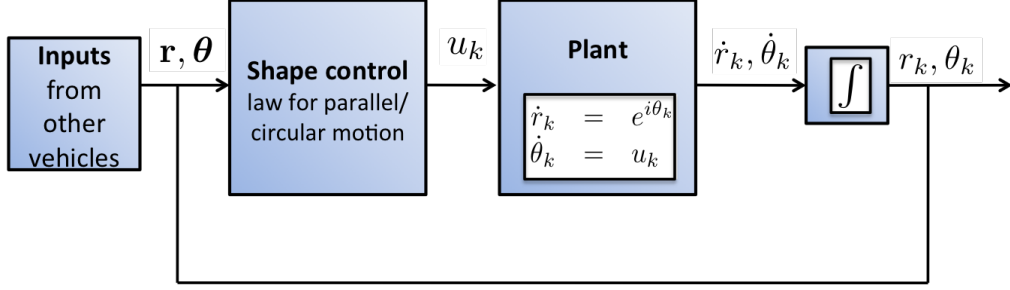


Figure 1.4: Block diagram for the first-order particle model.

k th vehicle in the plane about the z -axis is given by the matrix

$$R(\theta_k) = \begin{bmatrix} \cos \theta_k & -\sin \theta_k \\ \sin \theta_k & \cos \theta_k \end{bmatrix}, \quad (1.9)$$

a member of the rotation group $SO(2)$. If we denote $G(2)$ as the group of all 2×2 matrices, then $SO(2) = \{R \in G(2) \mid \det(R) = 1, R^T R = I\}$. The translation of a vehicle in the plane is given by the vector $p \in \mathbb{R}^2$, where $p = [x, y]^T$. Thus, we can describe the motion (rotational and translational) of a vehicle in the plane as $SE(2) = \mathbb{R}^2 \times SO(2)$, where “ \times ” denotes that we are taking the internal direct product of \mathbb{R}^2 and $SO(2)$ [25, 12].

In engineering applications that utilize a decentralized multi-agent network, sensing the absolute positions and orientations may be both costly and/or computationally burdensome. Thus, it is natural to seek motion coordination algorithms that use relative positions, orientations, and velocities as opposed to absolute variables [19]. In the inertial reference frame, the position and velocity orientation of each particle can be represented by the Euclidean group $SE(2)$. If we denote this group as G_k for the k th vehicle, then the configuration space may be designated as

$M_{config} = G_1 \times G_2 \times \cdots \times G_N$ for $k = 1, \dots, N$ [15]. Thus, M_{config} contains 3^N elements.

When relative positions and orientations are considered, the configuration space undergoes a reduction in the number of elements it contains; the shape space is thus expressed as M_{config}/G and contains $3N - 3$ degrees of freedom [15, 33]. The first-order controllers $\phi_{i,k}$, $i = 1, 2$ are each expressed in terms of shape variables, with the controller for parallel motion being expressed in terms of relative orientations $\eta_{3,j} - \eta_{3,k}$, and the controller for circular motion expressed in terms of relative positions $(r_k - r_j)e^{i\eta_{3,k}}$. Thus, under these controllers, we control the shape dynamics rather than the absolute dynamics of the system. The closed-loop dynamics of these first-order systems are invariant under the action of the symmetry group $SE(2)$ [33]. In other words, if the entire network were displaced or rotated, the closed-loop behavior of the particle model would not be affected.

1.3 Review of Parallel and Circular Formations

Parallel and circular formations have been determined by [15] as the only two relative equilibria of the configuration space. Parallel formations have the key control parameter p_θ defined as [33]

$$p_\theta = \frac{1}{N} \sum_{k=1}^N e^{i\theta_k}, \tag{1.10}$$

where p_θ represents the average linear momentum of the particles (assuming they have unit mass). Collective motion in a parallel formation is achieved by minimizing

the average linear momentum of the particle system via the phase potential [33]

$$V(\boldsymbol{\theta}) = \frac{1}{2}(1 - |p_\theta|^2), \quad (1.11)$$

where $\boldsymbol{\theta} = [\theta_1, \dots, \theta_N]^T$.

For the first-order system, the controller for parallel formations $\dot{\theta}_k = \phi_k(\boldsymbol{\theta})$ is [33]

$$\phi_k(\boldsymbol{\theta}) = -K \langle p_\theta, i e^{i\theta_k} \rangle, \quad K < 0. \quad (1.12)$$

The solutions θ_k converge to the largest invariant set for which $\dot{V} \equiv 0$, given by [33]

$$\Lambda = \{ \langle p_\theta, i e^{i\theta_k} \rangle \equiv 0 \forall k \}. \quad (1.13)$$

The condition that $\langle p_\theta, i e^{i\theta_k} \rangle \equiv 0$ implies that $\theta_j = \theta_k$ for all particle pairs j and k [33]. The condition that $\phi_k(\boldsymbol{\theta}) = 0$ in Λ implies that θ_k is constant for all k . Thus, Λ contains the set of parallel formations. All other formations in Λ are unstable [33].

Collective circular motion is achieved by minimizing the spacing potential [33]

$$V(\mathbf{r}, \boldsymbol{\theta}) = \frac{1}{2} \langle \mathbf{c}, P\mathbf{c} \rangle, \quad (1.14)$$

where $\mathbf{r} \equiv [r_1, \dots, r_N]^T$. The $N \times 1$ matrix \mathbf{c} contains the centers c_k , $k = 1, \dots, N$, of

the circular paths followed by each particle, where [33]

$$c_k = r_k + i\omega_0^{-1}e^{i\theta_k}. \quad (1.15)$$

$P = I_{N \times N} - \frac{1}{N}\mathbf{1}\mathbf{1}^T$ is an $N \times N$ matrix that projects onto the space orthogonal to $\mathbf{1} = [1, \dots, 1]^T \in \mathbb{R}^N$ and P_k represents the k th row of P . For the first-order system, the controller for circular formations is [33]

$$\phi_k(\mathbf{r}, \boldsymbol{\theta}) = \omega_0(1 + K\langle P_k\mathbf{c}, e^{i\theta_k} \rangle), K > 0. \quad (1.16)$$

The solutions θ_k converge to the largest invariant set Λ for which $\dot{V} \equiv 0$, given by [33]

$$\Lambda = \{\langle P_k\mathbf{c}, e^{i\theta_k} \rangle \equiv 0 \ \forall \ k\}. \quad (1.17)$$

$\langle P_k\mathbf{c}, e^{i\theta_k} \rangle = 0$ implies that $P_k\mathbf{c} = 0$, which is only true when all circular centers are the same; that is, $P_k\mathbf{c} = 0$ if and only if \mathbf{c} is in the span of $\mathbf{1}$. Thus we have $\dot{\theta}_k = \phi_k(\boldsymbol{\theta}) = \omega_0$. All N particles travel around the same circle of radius $1/|\omega_0|$ [27].

When a uniform, time-invariant flowfield is present, the first-order controller for parallel motion is given by [27]

$$\phi_k(\boldsymbol{\gamma}) = -K\langle p_\gamma, ie^{i\gamma_k} \rangle, K < 0, \quad (1.18)$$

where, similarly to the flow-free case, $p_\gamma = \frac{1}{N} \sum_{k=1}^N e^{i\gamma_k}$ represents the average linear momentum of the group. Likewise, the first-order controller for circular formations

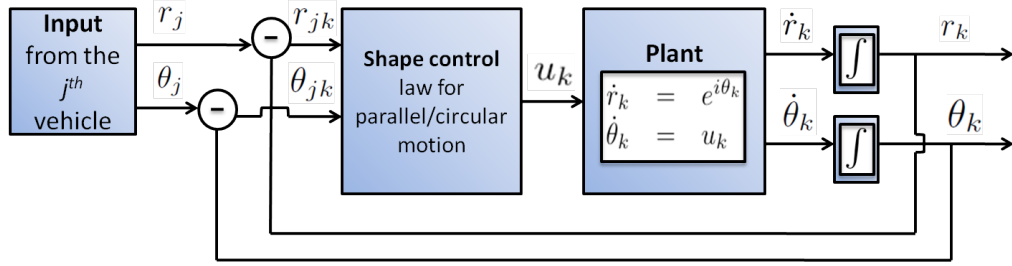


Figure 1.5: Block diagram for the first-order particle model in terms of shape variables.

in a flowfield is given by [27]

$$\phi_k(\mathbf{r}, \boldsymbol{\gamma}) = \omega_0(s_k + K \langle P_k \mathbf{c}, e^{i\boldsymbol{\gamma}_k} \rangle), K > 0. \quad (1.19)$$

For more details on these first-order controllers, the reader is directed to [27, 33, 15].

Chapter 2

Backstepping Control Design

2.1 Overview

Researchers began to utilize backstepping as a design tool in the late 1980s and early 1990s. Backstepping is a design technique developed for the stabilization of strict-feedback, nonlinear systems (that is, they have a lower-triangular structure) [17]. In a strict-feedback system of M states, the m th state, where $m = 1, 2, \dots, M$, is a function of the $1, \dots, m$ states, and contains none of the $m+1, \dots, M$ state variables. The state for which $m = M$ contains the control input, u [16]. This idea is more formally realized by the following example of a strict-feedback system [16]

$$\begin{aligned}\dot{\eta} &= f_0(\eta) + h_0(\eta)\eta_1 \\ \dot{\eta}_1 &= f_1(\eta, \eta_1) + h_1(\eta, \eta_1)\eta_2 \\ \dot{\eta}_2 &= f_2(\eta, \eta_1, \eta_2) + h_2(\eta, \eta_1, \eta_2)\eta_3 \\ &\cdot \\ &\cdot \\ &\cdot \\ \dot{\eta}_{M-1} &= f_{M-1}(\eta, \eta_1, \dots, \eta_{M-1}) + h_{M-1}(\eta, \eta_1, \dots, \eta_{M-1})\eta_M \\ \dot{\eta}_M &= f_M(\eta, \eta_1, \dots, \eta_M) + h_M(\eta, \eta_1, \dots, \eta_M)u.\end{aligned}\tag{2.1}$$

To illustrate the backstepping procedure, we begin by examining the simplest instance of (2.1), for which $M = 1$. It is given by [16]

$$\begin{aligned}\dot{\eta} &= f_0(\eta) + h_0(\eta)\xi \\ \dot{\xi} &= u\end{aligned}\tag{2.2}$$

where $\xi = \eta_1$, $u = \eta_2$, $f_1(\eta, \eta_1) = 0$, and $h_1(\eta, \eta_1) = 1$. In this system of M equations, the first equation denotes the original system of interest. We assume that there is a Lyapunov function V by which we prove that the control ξ stabilizes the η dynamics and we assume that $f_0 \rightarrow 0$ as time goes to infinity [16]. Although this subsystem is stable, it is part of the larger system (2.2), whose origin is stabilized by the control u . We assume that this control is unknown, and we use backstepping to find it.

Since we know that ξ stabilizes the subsystem formed by the first equation of (2.2), it becomes the desired controller in the higher-ordered system, which we rename ϕ . The first step of the backstepping procedure is to rearrange the system (2.2) so that it contains an error variable $z = \xi - \phi$, which is the difference between the actual controller (ξ) and the desired controller (ϕ). To express (2.2) in terms of z , we add and subtract $h_0(\eta)\phi$ from (2.2) and rearrange to obtain [16]

$$\begin{aligned}\dot{\eta} &= f_0(\eta) + h_0(\eta)\phi + h_0(\eta)z \\ \dot{z} &= \dot{\xi} - \dot{\phi} = u - \dot{\phi}.\end{aligned}\tag{2.3}$$

If we define a new variable $\nu = u - \dot{\phi}$, then (2.3) can be re-written as [16]

$$\begin{aligned}\dot{\eta} &= f_0(\eta) + h_0(\eta)\phi + h_0(\eta)z \\ \dot{z} &= \nu.\end{aligned}\tag{2.4}$$

Now (2.4) represents (2.2) expressed in terms of the error z and control ν . To determine what ν is, we use what is called a *composite* Lyapunov function, shown below as [16]

$$V_c = V + \frac{1}{2}z^2.\tag{2.5}$$

This Lyapunov function is “composite” because it is the sum of two positive semi-definite terms. The first, V , is the Lyapunov function used for (2.2) to show that ξ stabilizes the η dynamics. The second term is $\frac{1}{2}z^2$, by which we incorporate the newly formed error variable into the Lyapunov analysis. Taking the time-derivative of (2.5) gives

$$\dot{V}_c = \dot{V} + z\dot{z}.\tag{2.6}$$

Substituting $\eta_1 = \phi + z$ (for any instances of η_1 that may appear in \dot{V}) and ν for \dot{z} yields

$$\dot{V}_c = \dot{V} + z\nu.\tag{2.7}$$

Now the control ν can be chosen to achieve negative semi-definiteness in (2.7). The backstepping procedure culminates with using ν to find controller u by $u = \nu + \dot{\phi}$ [16].

2.2 Backstepping and the Particle Model

Now we relate this overview of backstepping to the particle model (1.3). Notice that if we re-write (1.3) as [16]

$$\begin{aligned}\dot{\eta}_k &= f(\eta_k) + h(\eta_k)\xi_k \\ \dot{\xi}_k &= a_k,\end{aligned}\tag{2.8}$$

where $\eta_k = [\eta_{1,k}, \eta_{2,k}, \eta_{3,k}]^T$, ξ_k represents the control input $\dot{\theta}_k$, a_k is the unknown second-order steering controller,

$$f(\eta_k) = \begin{bmatrix} \cos \eta_{3,k} \\ \sin \eta_{3,k} \\ 0 \end{bmatrix}, \quad \text{and} \quad h(\eta_k) = \begin{bmatrix} 0 \\ 0 \\ 1 \end{bmatrix},$$

then our system resembles (2.2). Let $\phi_k(\eta)$ be the desired control of the η dynamics, where $\eta = [\eta_1, \dots, \eta_N]^T$. Using the transformation $z_k = \xi_k - \phi_k(\eta)$, (2.8) may be rewritten as [16]

$$\begin{aligned}\dot{\eta}_k &= f(\eta_k) + h(\eta_k)\phi_k(\eta) + h(\eta_k)z_k \\ \dot{z}_k &= \nu_k,\end{aligned}\tag{2.9}$$

where $\nu_k = a_k - \dot{\phi}_k$ is the backstepping control. In the higher-ordered model (2.9), the variable z_k represents the difference between the actual controller and the desired controller of the lower-ordered system [32]. Model (1.8) can be expressed similarly.

The expression for a_k is found through the standard backstepping procedure

to achieve $\xi_k = \phi_k$. We derive a_k via the composite Lyapunov function [16]

$$V_c = V + \frac{1}{2} \sum_{k=1}^N z_k^2, \quad (2.10)$$

where V is the smooth potential [16] that must be minimized in order to achieve collective parallel or circular motion in the first-order system. The term $z_k = \xi_k - \phi_k$ is the error between the desired and actual first-order rotational dynamics. Taking the derivative of (2.10) along solutions of (1.3) gives

$$\dot{V}_c = \sum_{k=1}^N \left[\frac{\partial V}{\partial \eta_{3,k}} \dot{\eta}_{3,k} + z_k \dot{z}_k \right], \quad (2.11)$$

where $\dot{\eta}_{3,k} = \phi_k + z_k$ and $\dot{z}_k = \nu_k$ is a controller that we design to achieve $\dot{V}_c \leq 0$. The backstepping controller a_k is found by the transformation

$$a_k = \nu_k + \dot{\phi}_k. \quad (2.12)$$

Backstepping is particularly useful for the particle model (1.3) because control of parallel and circular formations has already been demonstrated using the appropriate inputs [33, 27]. Since the goal of the present work is to extend the parallel and circular formation control laws to a rigid body setting, backstepping enables us to achieve stabilization of higher-ordered dynamics (i.e., the regulation of angular acceleration rather than angular velocity), and thus gives us second-order controllers for parallel and circular formations. In the next chapter, we explore the process of transforming the first-order control laws for parallel and circular formations into

their second-order counterparts via backstepping.

Chapter 3

Control of Second-Order Rotational Dynamics via Backstepping

We now describe a backstepping control design for the flow-free particle model in order to achieve asymptotic convergence to either a synchronized (parallel) formation or a circular formation. Phase synchronization is attained when the average linear momentum of the collective motion is maximized, that is, when $\eta_{3,k} = \eta_{3,j}$ for all pairs j and k [33]. On the other hand, if each particle in model (1.3) is driven in a circular trajectory of radius $1/|\omega_0|$ by setting $\dot{\eta}_{3,k} = \omega_0$, group circular motion occurs when the centers of each particle's trajectory coincide [33].

3.1 Parallel Formation Control

Consider the model (1.3) with $\dot{\eta}_{3,k} = \phi_{1,k}(\eta)$. Assuming unit-mass particles, the average linear momentum is

$$p_\theta \triangleq \frac{1}{N} \sum_{j=1}^N e^{i\eta_{3,j}}.$$

A gradient control law for phase stabilization is [33]

$$\phi_{1,k}(\eta) = -K \langle p_\theta, i e^{i\eta_{3,k}} \rangle, \quad K < 0. \quad (3.1)$$

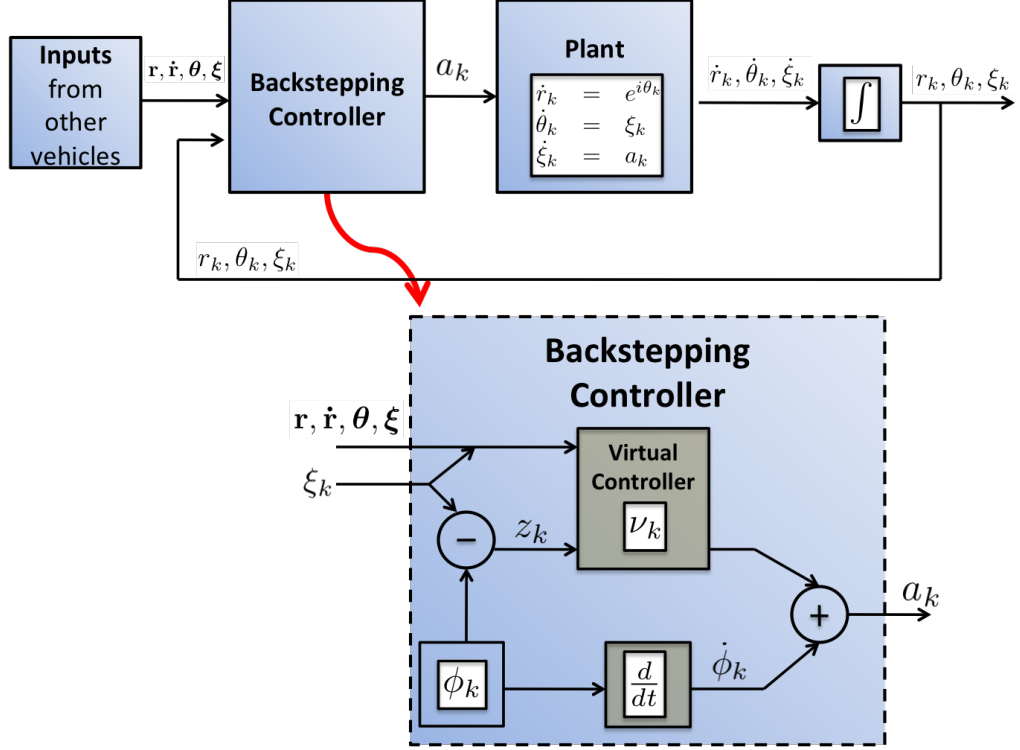


Figure 3.1: Block diagram for the second-order vehicle model.

The closed-loop behavior of the η dynamics with control $\phi_{1,k}(\eta)$ is established using the Lyapunov function [33]

$$V_1(\eta) = \frac{1}{2} \|p_\theta\|^2. \quad (3.2)$$

Taking the time derivative of $V_1(\eta)$, we obtain

$$\dot{V}_1 = \sum_{k=1}^N \frac{\partial V_1}{\partial \eta_{3,k}} \dot{\eta}_{3,k} = \frac{1}{N} \sum_{k=1}^N \langle p_\theta, i e^{i\eta_{3,k}} \rangle \dot{\eta}_{3,k}. \quad (3.3)$$

Substituting $\phi_{1,k}(\eta)$ into (3.3) yields

$$\dot{V}_1 = -\frac{K}{N} \sum_{k=1}^N \langle p_\theta, i e^{i\eta_{3,k}} \rangle^2 \geq 0.$$

According to [33, Theorem 1] the potential $V_1(\eta) = \frac{1}{2}\|p_\theta\|^2$ reaches its unique minimum when $p_\theta = 0$ (balancing) and its unique maximum when all phases are identical (synchronization). All other critical points of V_1 are isolated in the reduced space of relative phases (shape space) and are saddle points of V_1 . We are interested in stabilizing the set of synchronized critical points in the model (1.3), which are attained for the closed-loop η dynamics when $K < 0$.

Now we design a backstepping control for the higher-ordered system (1.3). We use the composite Lyapunov function

$$V_{1,c}(\eta, z) = -V_1(\eta) + \frac{1}{2} \sum_{k=1}^N z_k^2, \quad (3.4)$$

where $z_k = \xi_k - \phi_{1,k}(\eta)$, and $\phi_{1,k}(\eta)$ is given by (3.1). The time derivative of $V_{1,c}$ is

$$\dot{V}_{1,c} = \sum_{k=1}^N \left[-\frac{1}{N} \langle p_\theta, i e^{i\eta_{3,k}} \rangle \dot{\eta}_{3,k} + z_k \dot{z}_k \right]. \quad (3.5)$$

Substituting $\dot{z}_k = \nu_k$ and $\dot{\eta}_{3,k} = \phi_{1,k}(\eta) + z_k$ into (3.5) yields

$$\begin{aligned} \dot{V}_{1,c} &= \sum_{k=1}^N -\frac{1}{N} \langle p_\theta, i e^{i\eta_{3,k}} \rangle (\phi_{1,k}(\eta) + z_k) + z_k \nu_k \\ &= \sum_{k=1}^N -\frac{1}{N} \langle p_\theta, i e^{i\eta_{3,k}} \rangle (-K \langle p_\theta, i e^{i\eta_{3,k}} \rangle + z_k) + z_k \nu_k. \end{aligned} \quad (3.6)$$

Choosing

$$\nu_k = \frac{1}{N} \langle p_\theta, i e^{i\eta_{3,k}} \rangle - \kappa z_k, \quad \kappa > 0$$

gives

$$\dot{V}_{1,c} = \sum_{k=1}^N \left[\frac{K}{N} \langle p_\theta, i e^{i\eta_{3,k}} \rangle^2 - \kappa z_k^2 \right] \leq 0.$$

The control $a_k = \nu_k + \dot{\phi}_{1,k}$ that asymptotically stabilizes parallel formations in the model (1.3) is

$$\begin{aligned} a_k &= \frac{1}{N} \langle p_\theta, i e^{i\eta_{3,k}} \rangle - \kappa (\xi_k + K \langle p_\theta, i e^{i\eta_{3,k}} \rangle) \\ &\quad - \frac{K}{N} \sum_{j=1}^N [\langle e^{i\eta_{3,j}}, e^{i\eta_{3,k}} \rangle (\xi_j - \xi_k)], \quad K < 0, \end{aligned} \quad (3.7)$$

where $\dot{\phi}_{1,k}$ is obtained by taking the derivative of (3.1).

Theorem 1. *Consider the particle model (1.3) with the backstepping control (3.7). Under this control, the set of formations for which $\eta_{3,k} = \eta_{3,j}$ for all pairs j and k is asymptotically stable.*

Proof. $V_{1,c}$ is a smooth potential. By the invariance principle, we know that the solutions of (1.3) with the control (3.7) converge to the largest invariant set Λ for which $\dot{V}_{1,c} \equiv 0$, given by

$$\Lambda = \{ \langle p_\theta, i e^{i\eta_{3,k}} \rangle \equiv 0, z_k \equiv 0 \quad \forall k \}. \quad (3.8)$$

The condition that $\langle p_\theta, i e^{i\eta_{3,k}} \rangle = 0$ implies Λ contains parallel, balanced, and unbalanced motions; only parallel are stable for $K < 0$ [33]. $z_k = 0$ implies $\xi_k = \phi_{1,k}(\eta)$; however, from (3.1) we know that $\phi_{1,k}(\eta) = 0$ in Λ . This implies that $\eta_{3,k}$ is constant for all k . □

This result is illustrated in Fig. 3.2a, using $N = 16$, $K = -1$, and $\kappa = 5$.

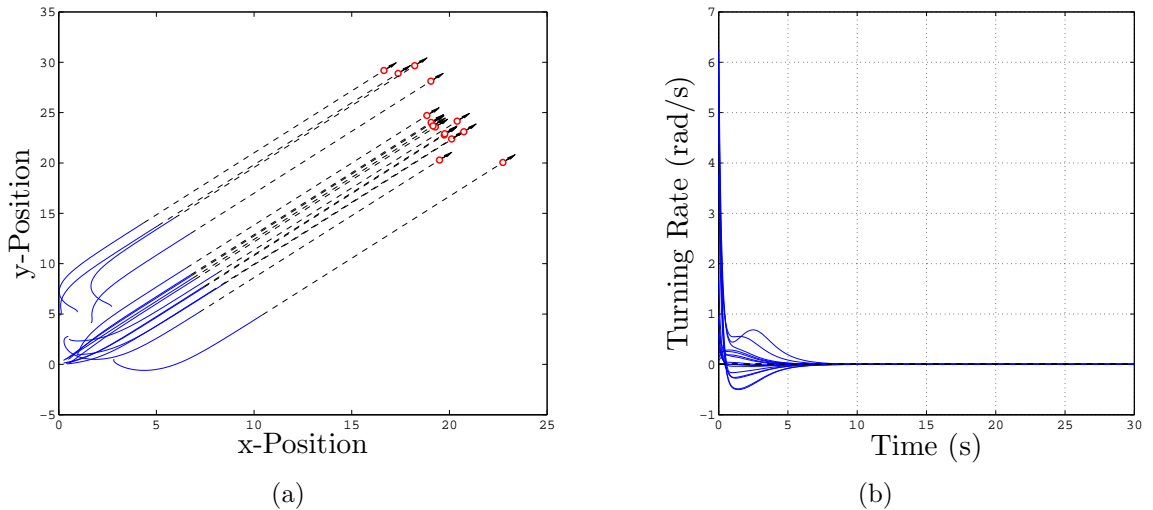


Figure 3.2: (a) Synchronized motion of self-propelled vehicles with second-order rotational dynamics. The dotted-line trajectories indicate that a parallel formation has been attained. (b) Turning rate of each vehicle, stabilized to zero using the backstepping-based controller. The vehicles have been randomly initialized.

3.2 Circular Formation Control

For the stabilization of circular formations, we again consider the model (1.3)

with $\dot{\eta}_{3,k} = \phi_{2,k}(\eta)$, where

$$\phi_{2,k}(\eta) = \omega_0(1 + K \langle P_k \mathbf{c}, e^{i\eta_{3,k}} \rangle), \quad K > 0. \quad (3.9)$$

Equation (3.9) represents a decentralized control law for the η dynamics that asymptotically stabilizes the set of circular formations [33]. The $N \times 1$ matrix \mathbf{c} contains the centers c_k , $k = 1, \dots, N$, of the circular paths followed by each of the particles k , where

$$c_k = r_k + i\omega_0^{-1} e^{i\eta_{3,k}}. \quad (3.10)$$

$P = I_{N \times N} - \frac{1}{N} \mathbf{1} \mathbf{1}^T$ is an $N \times N$ matrix that projects onto the space orthogonal to $\mathbf{1} = [1, \dots, 1]^T \in \mathbb{R}^N$ and P_k represents the k th row of P .

As in the case of synchronized motion, we begin our derivation of the circular formation control law by briefly reviewing the methods used by [33] to analyze the η dynamics. Consider the Lyapunov function [33]

$$V_2(\eta) = \frac{1}{2} \langle \mathbf{c}, P \mathbf{c} \rangle \quad (3.11)$$

whose derivative is

$$\dot{V}_2 = \sum_{k=1}^N \langle \dot{c}_k, P_k \mathbf{c} \rangle = \sum_{k=1}^N \langle e^{i\eta_{3,k}}, P_k \mathbf{c} \rangle (1 - \omega_0^{-1} \dot{\eta}_{3,k}).$$

If $\phi_{2,k}(\eta)$ is chosen to be the control (3.9), then the derivative of the Lyapunov function becomes [33]

$$\dot{V}_2 = -K \sum_{k=1}^N \langle P_k \mathbf{c}, e^{i\eta_{3,k}} \rangle^2 \leq 0.$$

By [33, Theorem 2] we know that the control $\phi_{2,k}(\eta)$ forces all solutions of the η dynamics to converge to the largest invariant set Λ , where [33]

$$\langle P_k \mathbf{c}, e^{i\eta_{3,k}} \rangle \equiv 0 \quad \forall k. \quad (3.12)$$

In Λ , $\dot{\eta}_{3,k} = \omega_0$ and $\dot{c}_k = 0$. The condition in (3.12) is met only when $P \mathbf{c} = 0$, which implies $c_k = c_j$ for all pairs j and k .

We use the Lyapunov function (3.11) to form the composite Lyapunov function

$$V_{2,c} = \frac{1}{2} \langle \mathbf{c}, P\mathbf{c} \rangle + \frac{1}{2} \sum_{k=1}^N z_k^2. \quad (3.13)$$

Taking the time-derivative along the solutions of (1.3), we obtain

$$\dot{V}_{2,c} = \sum_{k=1}^N \langle e^{i\eta_{3,k}}, P_k \mathbf{c} \rangle (1 - \omega_0^{-1} \dot{\eta}_{3,k}) + z_k \dot{z}_k.$$

Using $\dot{z}_k = \nu_k$ and $\dot{\eta}_{3,k} = \phi_{2,k}(\eta) + z_k$, $\dot{V}_{2,c}$ becomes

$$\begin{aligned} \dot{V}_{2,c} &= \sum_{k=1}^N \langle e^{i\eta_{3,k}}, P_k \mathbf{c} \rangle (1 - \omega_0^{-1} (\phi_{2,k}(\eta) + z_k)) + z_k \nu_k \\ &= \sum_{k=1}^N -K \langle P_k \mathbf{c}, e^{i\eta_{3,k}} \rangle^2 - \omega_0^{-1} \langle P_k \mathbf{c}, e^{i\eta_{3,k}} \rangle z_k + z_k \nu_k. \end{aligned}$$

Choosing

$$\nu_k = -\kappa z_k + \omega_0^{-1} \langle P_k \mathbf{c}, e^{i\eta_{3,k}} \rangle$$

yields

$$\dot{V}_{2,c} = \sum_{k=1}^N -K \langle P_k \mathbf{c}, e^{i\eta_{3,k}} \rangle^2 - \kappa z_k^2 \leq 0.$$

If we use the transformation $a_k = v_k + \dot{\phi}_{2,k}$ and define the quantity $\tilde{r}_k = r_k - \frac{1}{N} \sum_{j=1}^N r_j$, then the second-order controller for circular motion can be written as

$$\begin{aligned} a_k &= -\kappa (\xi_k - \phi_{2,k}(\eta)) + \omega_0 K \xi_k \langle \tilde{r}_k, i e^{i\eta_{3,k}} \rangle \\ &\quad + K \left(\omega_0 - \frac{1}{N} \sum_{j=1}^N [\langle e^{i\eta_{3,j}}, e^{i\eta_{3,k}} \rangle (\omega_0 - (\xi_j - \xi_k))] \right) \\ &\quad + \omega_0^{-1} \left(\langle \tilde{r}_k, e^{i\eta_{3,k}} \rangle - \omega_0^{-1} \frac{1}{N} \sum_{j=1}^N \langle i e^{i\eta_{3,j}}, e^{i\eta_{3,k}} \rangle \right). \end{aligned} \quad (3.14)$$

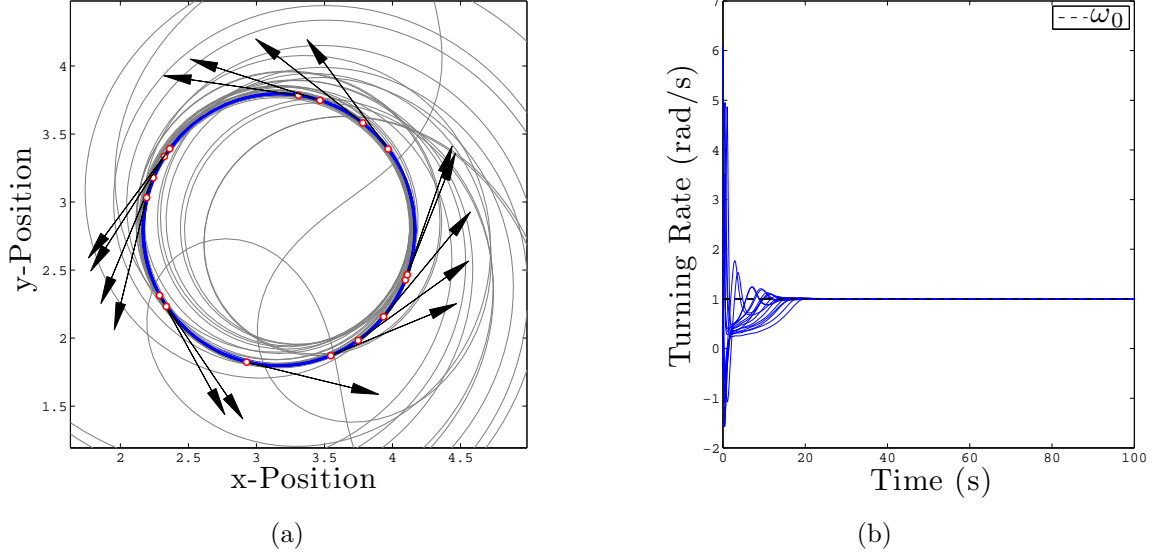


Figure 3.3: (a) Stabilization of a circular formation of self-propelled vehicles with second-order rotational dynamics. (b) The steady-state turning rate of each vehicle is $\omega_0 = 1$. The vehicles have been randomly initialized.

Theorem 2. *Consider the particle model (1.3) with the backstepping control (3.14). All solutions converge to the set of circular formations with radius $1/|\omega_0|$ and the direction of rotation determined by the sign of ω_0 .*

Proof. By the invariance principle, we know that the solutions of (1.3) with the control (3.14) converge to the largest invariant set Λ for which $\dot{V}_{2,c} \equiv 0$, given by

$$\Lambda = \{ \langle P_k \mathbf{c}, e^{i\eta_{3,k}} \rangle \equiv 0, z_k \equiv 0 \ \forall \ k \}. \quad (3.15)$$

$\langle P_k \mathbf{c}, e^{i\eta_{3,k}} \rangle = 0$ implies that $P_k \mathbf{c} = 0$, which is only true when all circular centers are the same; that is, $P_k \mathbf{c} = 0$ if and only if \mathbf{c} is in the span of $\mathbf{1}$. Using (3.9) along with the fact that $\langle P_k \mathbf{c}, e^{i\eta_{3,k}} \rangle = z_k = 0$, we have $\dot{\eta}_{3,k} = \phi_{2,k}(\eta) = \omega_0$. Thus, all N

particles travel around the same circle of radius $1/|\omega_0|$. □

This result is illustrated in Fig. 3.3a, where $N = 16$, $K = 1$, $\kappa = 5$, and $\omega_0 = 1$.

Chapter 4

Control of Second-Order Rotational Dynamics in a Uniform Flowfield

We now design a backstepping control considering a uniform, time-invariant flowfield. In a flowfield, phase synchronization is attained when the inertial phase angles satisfy $\tau_{3,k} = \tau_{3,j}$ for all pairs j and k . Group circular motion occurs under the control $\dot{\tau}_{3,k} = \omega_0 s_k$, when the centers of all particle trajectories coincide [27]. We require that each vehicle know the local flowfield.

4.1 Parallel Formation Control

The model for a particle traveling in a uniform, time-invariant flowfield is given by (1.8), where $\dot{\tau}_{3,k} = \phi_{3,k}(\tau)$. We show that the set of parallel formations is stabilized by the control [27]

$$\phi_{3,k}(\tau) = -K \langle p_\gamma, i e^{i\tau_{3,k}} \rangle, \quad (4.1)$$

where $K < 0$. This is proven using the Lyapunov function

$$V_3(\tau) = \frac{1}{2} \|p_\gamma\|^2, \quad (4.2)$$

which we seek to maximize in order to achieve phase synchronization. Similarly to p_θ in the flow-free case, p_γ is defined as the average inertial linear momentum, i.e.,

$$p_\gamma = \frac{1}{N} \sum_{j=1}^N e^{i\tau_{3,j}}.$$

The time-derivative of the Lyapunov function (4.2) is

$$\dot{V}_3 = \sum_{k=1}^N \frac{\partial V_3}{\partial \tau_{3,k}} \dot{\tau}_{3,k} = \frac{1}{N} \sum_{k=1}^N \langle p_\gamma, i e^{i\tau_{3,k}} \rangle \phi_{3,k}(\tau).$$

With $\phi_{3,k}(\tau)$ given by (4.1), the derivative of the Lyapunov function becomes

$$\dot{V}_3 = \sum_{k=1}^N -\frac{K}{N} \langle p_\gamma, i e^{i\tau_{3,k}} \rangle^2 \geq 0.$$

From [27, Theorem 1] we know that all solutions converge to the critical set of V_3 .

With $K < 0$, the set of synchronized motions are asymptotically stable and every other equilibrium is unstable.

We use this result to derive the phase stabilization control law for the higher-ordered system. The composite Lyapunov function is

$$V_{3,c}(\tau, z) = -V_3(\tau) + \frac{1}{2} \sum_{k=1}^N z_k^2,$$

where $z_k = \Omega_k - \phi_{3,k}(\tau)$. The time derivative of the composite Lyapunov function yields

$$\dot{V}_{3,c} = \sum_{k=1}^N \left[-\frac{1}{N} \langle p_\gamma, i e^{i\tau_{3,k}} \rangle \dot{\tau}_{3,k} + z_k \dot{z}_k \right].$$

Using $\dot{z}_k = \nu_k$ and $\dot{\tau}_{3,k} = \phi_{3,k}(z) + z_k$, the derivative becomes

$$\begin{aligned}\dot{V}_{3,c} &= \sum_{k=1}^N \left[-\frac{1}{N} \langle p_\gamma, ie^{i\tau_{3,k}} \rangle (\phi_{3,k}(\tau) + z_k) + z_k \nu_k \right] \\ &= \sum_{k=1}^N \left[-\frac{1}{N} \langle p_\gamma, ie^{i\tau_{3,k}} \rangle (-K \langle p_\gamma, ie^{i\tau_{3,k}} \rangle + z_k) + z_k \nu_k \right].\end{aligned}$$

Choosing

$$\nu_k = \frac{1}{N} \langle p_\gamma, ie^{i\tau_{3,k}} \rangle - \kappa z_k, \quad \kappa > 0$$

gives

$$\dot{V}_{3,c} = \sum_{k=1}^N \left[\frac{K}{N} \langle p_\gamma, ie^{i\tau_{3,k}} \rangle^2 - \kappa z_k^2 \right] \leq 0.$$

Using the transformation $\lambda_k = \nu_k + \dot{\phi}_k$, the control may be written as

$$\begin{aligned}\lambda_k &= \frac{1}{N} \langle p_\gamma, ie^{i\tau_{3,k}} \rangle - \kappa (\Omega_k + K \langle p_\gamma, ie^{i\tau_{3,k}} \rangle) \\ &\quad - \frac{K}{N} \sum_{j=1}^N [\langle e^{i\tau_{3,j}}, e^{i\tau_{3,k}} \rangle (\Omega_j - \Omega_k)], \quad K < 0.\end{aligned}\tag{4.3}$$

Theorem 3. *Consider the particle model (1.8) with the backstepping control (4.3) and flow $f_k = \alpha < 1$. For $K < 0$ the set of formations where $\tau_{3,k} = \tau_{3,j}$ for all pairs j and k is asymptotically stable.*

The proof for parallel motion in the presence of a time-invariant flowfield follows the proof given for Theorem 1, with $\eta_{3,k}$ replaced by $\tau_{3,k}$ and ξ_k replaced by Ω_k . This result is illustrated in Fig. 4.1a, using $N = 16$, $K = -1$, $\kappa = 5$.

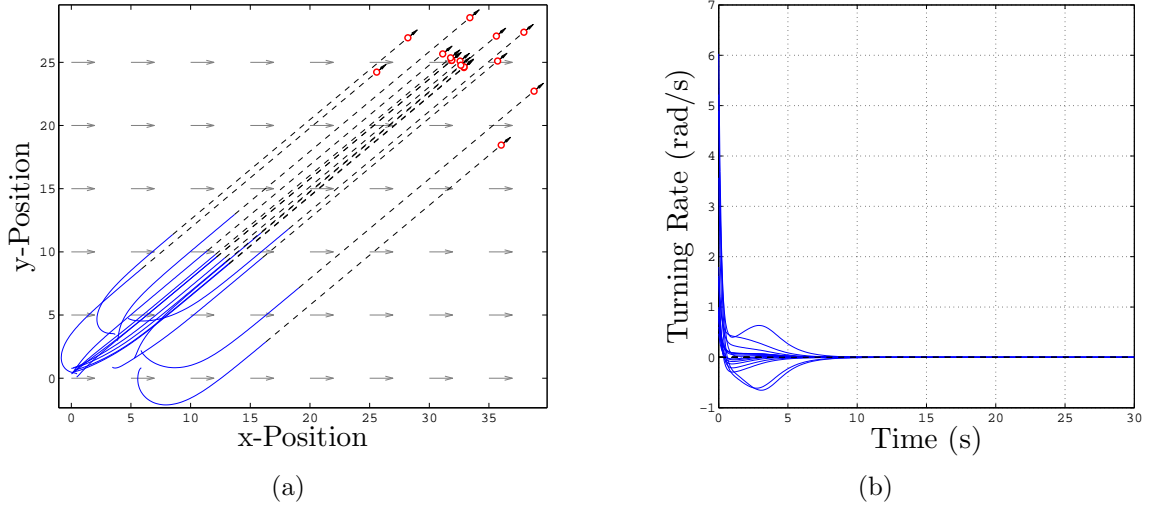


Figure 4.1: (a) Stabilization of a parallel formation in a uniform, time-invariant flowfield $\alpha = 0.5$. (b) Turning rate of each vehicle, stabilized to zero using the backstepping-based controller. Randomly-generated initial conditions.

4.2 Circular Formation Control

For collective motion control of circular formations in a time-invariant flowfield, we consider the model (1.8) with $\dot{\tau}_{3,k} = \phi_{4,k}(\tau)$, where

$$\phi_{4,k}(\tau) = \omega_0(s_k + K\langle P_k \mathbf{c}, e^{i\tau_{3,k}} \rangle) \quad (4.4)$$

and $K > 0$. Similarly to the flow-free case, the center of each particle's trajectory is given by $c_k = r_k + i\omega_0^{-1}e^{i\tau_{3,k}}$, and the radius of the circular trajectory is given by $1/|\omega_0|$ [27]. We reiterate the stability analysis of [27] to show that the spacing control $\phi_{4,k}(\tau)$ asymptotically stabilizes the set of circular formations. This is proven using the Lyapunov function

$$V_4(\tau) = \frac{1}{2}\langle \mathbf{c}, P\mathbf{c} \rangle, \quad (4.5)$$

which has the time derivative

$$\begin{aligned}\dot{V}_4 &= \sum_{k=1}^N \langle \dot{c}_k, P_k \mathbf{c} \rangle \\ &= \sum_{k=1}^N \langle P_k \mathbf{c}, e^{i\tau_{3,k}} \rangle (s_k - \omega_0^{-1} \phi_{4,k}(\tau)).\end{aligned}$$

Substituting $\phi_{4,k}(\tau)$ from (4.4) gives

$$\dot{V}_4 = -\sum_{k=1}^N K \langle P_k \mathbf{c}, e^{i\tau_{3,k}} \rangle^2 \leq 0.$$

As stated in [27, Theorem 3], the control (4.4) forces the convergence of all solutions of the τ dynamics in (1.8) to the largest invariant set Λ of V_4 , in which

$$\langle P_k \mathbf{c}, e^{i\tau_{3,k}} \rangle \equiv 0. \quad (4.6)$$

In Λ , $\dot{\tau}_{3,k} = \omega_0 s_k$ and $\dot{c}_k = 0$. Therefore, the condition (4.6) is met only when $P \mathbf{c} = 0$, which implies that $c_k = c_j$ for all pairs j and k .

Using (4.5) we form the composite Lyapunov function

$$V_{4,c}(\tau, z) = V_4(\tau) + \frac{1}{2} \sum_{k=1}^N z_k^2$$

whose derivative along solutions of (1.8) is

$$\dot{V}_{4,c} = \sum_{k=1}^N \langle P_k \mathbf{c}, e^{i\tau_{3,k}} \rangle (s_k - \omega_0^{-1} \dot{\tau}_{3,k}) + z_k \dot{z}_k.$$

Making the substitutions $\dot{z}_k = \nu_k$ and $\dot{\tau}_{3,k} = \phi_{4,k}(\tau) + z_k$, we rewrite the time

derivative as

$$\begin{aligned}\dot{V}_{4,c} &= \sum_{k=1}^N \langle P_k \mathbf{c}, e^{i\tau_{3,k}} \rangle (s_k - \omega_0^{-1} (\phi_{4,k}(\tau) + z_k)) + z_k \nu_k \\ &= \sum_{k=1}^N -K \langle P_k \mathbf{c}, e^{i\tau_{3,k}} \rangle^2 - \omega_0^{-1} \langle P_k \mathbf{c}, e^{i\tau_{3,k}} \rangle z_k + z_k \nu_k.\end{aligned}\quad (4.7)$$

Choosing the control ν_k to be

$$\nu_k = -\kappa z_k + \omega_0^{-1} \langle P_k \mathbf{c}, e^{i\tau_{3,k}} \rangle,$$

yields

$$\dot{V}_{4,c} = \sum_{k=1}^N -K \langle P_k \mathbf{c}, e^{i\tau_{3,k}} \rangle^2 - \kappa z_k^2 \leq 0.$$

The control may be transformed into λ_k using the transformation $\lambda_k = \nu_k + \dot{\phi}_{4,k}$.

Thus,

$$\begin{aligned}\lambda_k &= -\kappa(\Omega_k - \phi_{4,k}(\tau)) + \omega_0 K \Omega_k \langle \tilde{r}_k, i e^{i\tau_{3,k}} \rangle + \omega_0 \dot{s}_k \\ &\quad + K \left(\omega_0 s_k - \frac{1}{N} \sum_{j=1}^N [\langle e^{i\tau_{3,j}}, e^{i\tau_{3,k}} \rangle (\omega_0 s_j - (\Omega_j - \Omega_k))] \right) \\ &\quad + \omega_0^{-1} \left(\langle \tilde{r}_k, e^{i\tau_{3,k}} \rangle - \omega_0^{-1} \frac{1}{N} \sum_{j=1}^N \langle i e^{i\tau_{3,j}}, e^{i\tau_{3,k}} \rangle \right),\end{aligned}\quad (4.8)$$

where $\phi_{4,k}(\tau)$ is given by (4.4) and

$$\dot{s}_k = -\alpha \sin \tau_{3,k} \left[1 + \frac{\alpha \cos \tau_{3,k}}{\sqrt{1 - \alpha^2 \sin^2 \tau_{3,k}}} \right] \Omega_k.\quad (4.9)$$

Theorem 4. *Consider the particle model (1.8) with the backstepping control (4.8)*

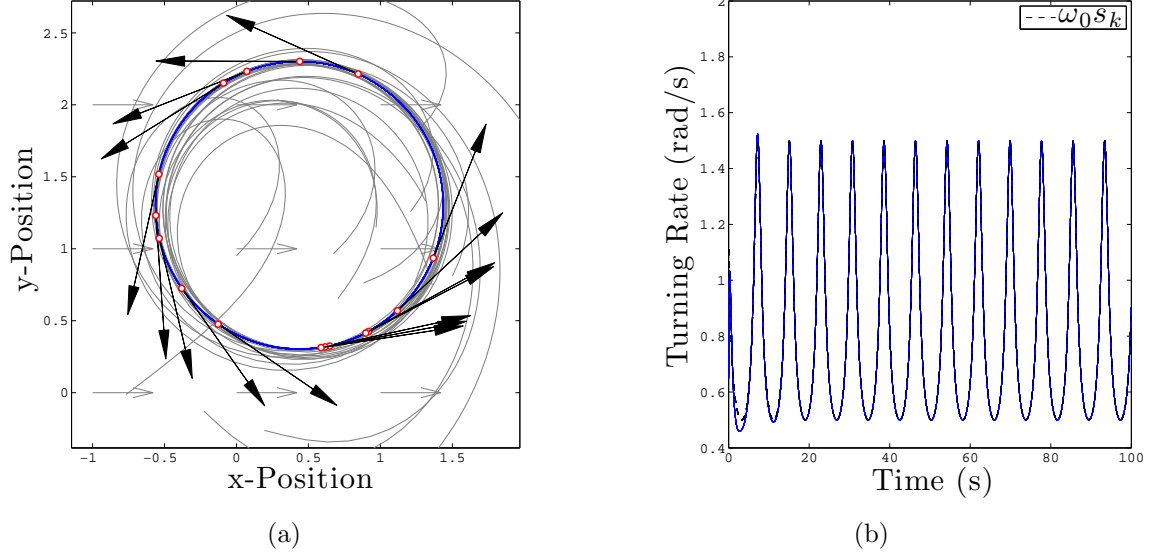


Figure 4.2: (a) Stabilization of a circular formation in a uniform, time-invariant flowfield $\alpha = 0.5$. (b) The steady-state turning rate of each vehicle is $\omega_0 = 1$ (shown for only one vehicle). Randomly-generated initial conditions.

and flow $f_k = \alpha < 1$. All solutions converge to the set of circular formations of radius $1/|\omega_0|$ and direction of rotation determined by the sign of ω_0 .

Proof. By the invariance principle, we know that the solutions of (1.8) with the control (4.8) converge to the largest invariant set Λ for which $\dot{V}_{4,c} \equiv 0$, given by

$$\Lambda = \{ \langle P_k \mathbf{c}, e^{i\tau_{3,k}} \rangle \equiv 0, z_k \equiv 0 \forall k \} \quad (4.10)$$

The first condition implies that $P_k \mathbf{c} = 0$, which is only true when all circular centers are the same. The second condition implies that $\Omega_k = \phi_{4,k}(\tau)$; thus, we have $\Omega_k = \phi_{4,k}(\tau) = \omega_0 s_k$. \square

This result is illustrated in Fig. 4.2a, with $N = 16$, $K = 1$, $\kappa = 5$, $\omega_0 = 1$.

Chapter 5

Considerations for Implementing the Backstepping Control

When using the control framework outlined in Chapters 3 and 4 for a collection of autonomous vehicles, several considerations should be taken into account in order to ensure that the controllers developed are compatible with the sensing, communication, and control hardware onboard each vehicle. In this chapter, several of these considerations are examined and addressed.

5.1 Computing the Steering Control for Vehicles in a Flowfield

Although deriving the control λ_k using (1.8) is useful in the backstepping design, implementing control model (1.7) onboard an aircraft or submarine requires an additional calculation. Model (1.8) considers the inertial angular velocity of the vehicle, while the yaw-control commands a_k for an aircraft are, in practice, given in terms of the angular velocity in the aircraft's body frame. Therefore, in order to derive a_k from λ_k , the following transformation is used. We begin with the transformation of the first-order control w_k in (1.5) to u_k in model (1.4) [27]

$$u_k = \frac{w_k - \langle f'_k, i \rangle}{1 - s_k^{-1} \langle e^{i\gamma_k}, f_k \rangle}. \quad (5.1)$$

Note that $f'_k = \partial f_k / \partial r_k$ and we have assumed a time-invariant flowfield. We extend these results to the second-order rotational dynamics by taking the time-derivative of (5.1) to obtain

$$\begin{aligned} \frac{d}{dt} \left(\frac{w_k - \langle f'_k, i \rangle}{1 - s_k^{-1} \langle e^{i\gamma_k}, f_k \rangle} \right) &= \frac{(1 - s_k^{-1} \langle e^{i\gamma_k}, f_k \rangle) (\dot{w}_k - \langle \dot{f}'_k, i \rangle)}{(1 - s_k^{-1} \langle e^{i\gamma_k}, f_k \rangle)^2} - \left(\frac{(w_k - \langle f'_k, i \rangle) s_k^{-2} \langle e^{i\gamma_k}, f_k \rangle \dot{s}_k}{(1 - s_k^{-1} \langle e^{i\gamma_k}, f_k \rangle)^2} \right. \\ &\quad \left. - \frac{(w_k - \langle f'_k, i \rangle) s_k^{-1} (\langle i e^{i\gamma_k}, f_k \rangle \dot{\gamma}_k + \langle e^{i\gamma_k}, \dot{f}_k \rangle)}{(1 - s_k^{-1} \langle e^{i\gamma_k}, f_k \rangle)^2} \right), \end{aligned} \quad (5.2)$$

where \dot{s}_k is defined in (4.9), $\dot{f}_k = f'_k \dot{r}_k$, and $\dot{f}'_k = \frac{d}{dt} \left(\frac{\partial f_k}{\partial r_k} \right)$. Using $\lambda_k = \dot{w}_k$, this transformation simplifies to

$$a_k = \frac{\lambda_k - \langle \dot{f}'_k, i \rangle}{1 - s_k^{-1} \langle e^{i\gamma_k}, f_k \rangle} - \left(\frac{(w_k - \langle f'_k, i \rangle) [s_k^{-2} \langle e^{i\gamma_k}, f_k \rangle \dot{s}_k - s_k^{-1} \langle i e^{i\gamma_k}, f_k \rangle \dot{\gamma}_k - s_k^{-1} \langle e^{i\gamma_k}, \dot{f}_k \rangle]}{(1 - s_k^{-1} \langle e^{i\gamma_k}, f_k \rangle)^2} \right). \quad (5.3)$$

When we consider $f_k = \alpha$, then (5.3) becomes

$$a_k = \frac{\lambda_k}{1 - s_k^{-1} \alpha \cos \gamma_k} - \frac{w_k \alpha \cos \gamma_k \dot{s}_k}{(s_k - \alpha \cos \gamma_k)^2} - \frac{w_k^2 \alpha \sin \gamma_k}{s_k (1 - s_k^{-1} \alpha \cos \gamma_k)^2}. \quad (5.4)$$

Eqs. (5.3) and (5.4) provide a control for model (1.7) as a function of λ_k , thus enabling us to implement the backstepping algorithm in practice.

5.2 Sensing and Communication Requirements

In this section, we focus on the sensing requirements for each vehicle under the backstepping controllers derived previously. As shown in Chapters 3 and 4, the backstepping procedure nearly preserves the results of the first-order stability

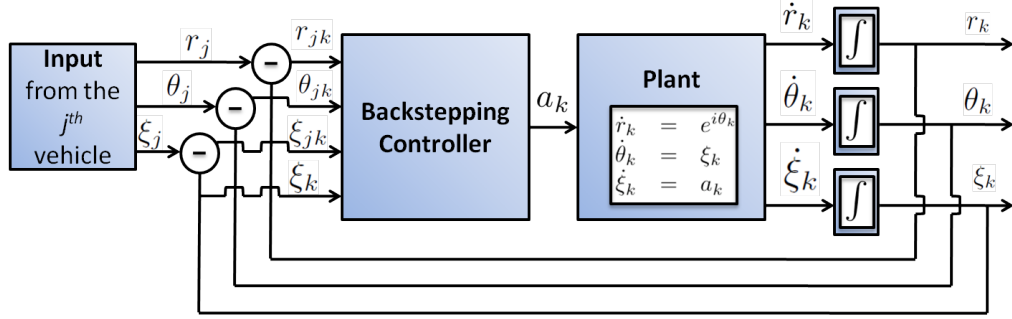


Figure 5.1: Block diagram for the second-order vehicle model in terms of shape variables.

analysis, with one difference being that the angular acceleration is regulated. When the angular acceleration is added to the state model, M_{config} contains 4^N elements, and the shape space has $4N - 4$ degrees of freedom.

Similar to their first-order counterparts, each backstepping-based control of the flow-free model has the desirable properties of a shape control. However, in order to implement (3.7) and (3.14), additional sensing requirements must be met. Note that the angular rate ξ_k appears alone, which introduces an additional sensing requirement for each vehicle: the yaw rate. Another sensing requirement is introduced when a flowfield is considered; each vehicle must know the components of the local flowfield along and across its direction of motion.

5.3 Comparison to Proportional Control

Since proportional control is widely used in engineering applications and simple to understand [2], we compare backstepping to a proportional control law. We analyze the performance of the proportional controller (5.5) in comparison to the backstepping controller for the case of parallel formations in the absence of a flow-

field. The results of the analysis for circular formations follows similarly. Consider the model (1.3), with the proportional controller

$$a_k = -K_p z_k, \quad (5.5)$$

where $z_k = \xi_k - \phi_k(\eta)$. We show that $|z_k|$ has a bound that can be reduced by increasing the proportional gain K_p . Analysis of saturation effects for the second-order model is the subject of ongoing work; analysis of saturation of the first-order model is available in [29].

Theorem 5. *Consider the Lyapunov function (3.4), for which $V_{1,c}(\eta, 0) = 0$ when $\eta_{3,k} = \eta_{3,j}$ and $V_{1,c}(\eta, z) \geq 0$ for all η and z . Under the controller (5.5),*

$$\dot{V}_{1,c} \leq 0 \text{ for all } |z_k| \geq \frac{1}{K_p} \left(\frac{1}{N} + \frac{|K|}{N} \sum_{j=1}^N |\xi_j - \xi_k| \right). \quad (5.6)$$

Proof. We substitute the proportional controller (5.5) into the equation $\nu_k = a_k - \dot{\phi}_{1,k}$ to obtain

$$\nu_k = -K_p z_k + \frac{K}{N} \sum_{j=1}^N \langle e^{i\eta_{3,j}}, e^{i\eta_{3,k}} \rangle (\xi_j - \xi_k). \quad (5.7)$$

Substituting this result into the derivative of the composite Lyapunov function, $\dot{V}_{1,c}$, given in (3.6), yields

$$\begin{aligned} \dot{V}_{1,c} = & \sum_{k=1}^N \left(\frac{K}{N} \langle p_\theta, i e^{i\eta_{3,k}} \rangle^2 + \right. \\ & \left. \left[-\frac{1}{N} \langle p_\theta, i e^{i\eta_{3,k}} \rangle + \frac{K}{N} \sum_{j=1}^N (\langle e^{i\eta_{3,j}}, e^{i\eta_{3,k}} \rangle (\xi_j - \xi_k)) \right] z_k - K_p z_k^2 \right). \end{aligned} \quad (5.8)$$

Note that (5.8) is quadratic in z_k , the difference between the desired and actual angular rates. In order to determine the values of z_k for which $\dot{V}_{1,c}$ is negative semi-definite, we begin by determining bounds for each of the coefficients in the quadratic expression given by (5.8). The first term $\frac{K}{N} \langle p_\theta, ie^{i\eta_{3,k}} \rangle^2$ is never positive and may be ignored. In order to capture the worst-case error, we establish an upper bound on z_k using the remaining terms as follows. We have

$$\begin{aligned} \dot{V}_{1,c} &\leq \sum_{k=1}^N \left(\left[-\frac{1}{N} \langle p_\theta, ie^{i\eta_{3,k}} \rangle + \frac{K}{N} \sum_{j=1}^N \langle e^{i\eta_{3,j}}, e^{i\eta_{3,k}} \rangle (\xi_j - \xi_k) \right] z_k - K_p z_k^2 \right) \\ &\leq \sum_{k=1}^N \left(\left[\frac{1}{N} + \frac{|K|}{N} \sum_{j=1}^N |\xi_j - \xi_k| \right] - K_p |z_k| \right) |z_k|, \end{aligned} \tag{5.9}$$

which yields the result (5.6). □

Although under the chosen Lyapunov function the controller (5.5) guarantees the error to be bounded according to (5.6), complete elimination of steady-state error with this controller cannot be established using (3.4). (Note that in simulation, zero steady-state error has been attained using the proportional controller and moderate gains, although analytically there is no guarantee of error elimination.) The difference in performance when using the backstepping-based controller is that it guarantees asymptotic convergence of the error dynamics to zero. Analysis of the efficacy of the proportional controller using a different Lyapunov function is given in [26].

Chapter 6

Extension to Planar Rigid-Body Dynamics

Recall that an existing idealized vehicle model for planar collective motion with second-order rotational dynamics is

$$\begin{aligned}\dot{r}_k &= e^{i\theta_k} \\ \dot{\theta}_k &= \omega_k \\ \dot{\omega}_k &= a_k,\end{aligned}\tag{6.1}$$

where a_k represents the second-order steering control of vehicle $k = 1, \dots, N$. Instead of the symbol ξ_k , we now use ω_k to denote the angular velocity of the k th vehicle. In this model each vehicle moves at unit speed in the direction θ_k . Model (6.1) represents an extension of a self-propelled particle model with first-order rotational dynamics [22]. In the first-order case, phase and spacing potentials were used to derive control laws for parallel and circular formations in the absence of an external flowfield [33], and in the presence of a spatiotemporal flowfield [29]. Since first-order rotational dynamics may not adequately describe rigid-body motion, these first-order particle models were used as the first component of a second-order system for which we designed controllers using integrator backstepping.

The expression for a_k is found through the standard backstepping procedure to achieve $\omega_k = \phi_k$, where ϕ_k is the steering controller used to generate parallel

and circular formations in the first-order system. We derive a_k via the composite Lyapunov function [16]

$$V_c = V + \frac{1}{2} \sum_{k=1}^N z_k^2, \quad (6.2)$$

where V is the smooth potential that must be minimized in order to achieve collective parallel or circular motion in the first-order system. The term $z_k = \omega_k - \phi_k$ is the error between the desired and actual first-order rotational dynamics. Taking the derivative of (6.2) along solutions of (6.1) gives

$$\dot{V}_c = \sum_{k=1}^N \left[\frac{\partial V}{\partial \theta_k} \dot{\theta}_k + z_k \dot{z}_k \right], \quad (6.3)$$

where $\dot{\theta}_k = \phi_k + z_k$ and $\dot{z}_k = \nu_k$ is a controller that we design to achieve $\dot{V}_c \leq 0$. The backstepping controller a_k is found by the transformation [16]

$$a_k = \nu_k + \dot{\phi}_k. \quad (6.4)$$

When a uniform, time-invariant flowfield is present, the second-order model (6.1) can be written as [22]

$$\begin{aligned} \dot{r}_k &= e^{i\theta_k} + f_k \\ \dot{\theta}_k &= \omega_k \\ \dot{\omega}_k &= a_k, \end{aligned} \quad (6.5)$$

where $f_k \in \mathbb{C}$ is the flowfield. This model can also be expressed more succinctly using the magnitude $s_k = |e^{i\theta_k} + f_k|$ and orientation $\gamma_k = \arg\{e^{i\theta_k} + f_k\}$ of the

inertial velocity [27]:

$$\begin{aligned}
 \dot{r}_k &= s_k e^{i\gamma_k} \\
 \dot{\gamma}_k &= \omega_k \\
 \dot{\omega}_k &= \lambda_k.
 \end{aligned}
 \tag{6.6}$$

While models (6.1) and (6.6) are useful for understanding the movement of particles in the plane, they may not be sufficient for describing rigid-body dynamics. The inclusion of second-order rotational dynamics is only a part of the transformation process from particle model to rigid-body model. In order to complete the transformation, in the next section we consider second-order translational dynamics as well.

Our goal is to develop a set of differential equations for the dynamic behavior of a collection of autonomous vehicles. We assume that each vehicle can translate in any combination of forward and transverse dynamics, and that rotational dynamics are governed by steering controllers. To relate the particle kinematics, in which the heading was expressed as an exponential, to a more standard kinematic model expressed in terms of unit vectors, recall that in model (6.1) each particle moves with unit forward speed and its direction of travel is determined by θ_k . Here we use θ_k to describe the orientation of a planar rigid body. With this description, $e^{i\theta_k} = \bar{x}_k$ defines the body-fixed reference frame $\mathcal{B}_k = (k, \bar{x}_k, \bar{y}_k, \bar{z}_k)$, where \bar{z}_k is out of the plane and $\bar{y}_k = \bar{z}_k \times \bar{x}_k$.

Let $u_k \in \mathbb{R}$ represent the forward speed of the k th vehicle in \mathcal{B}_k and $v_k \in \mathbb{R}$ the transverse speed. In this case, the k th velocity expressed as components in \mathcal{B}_k

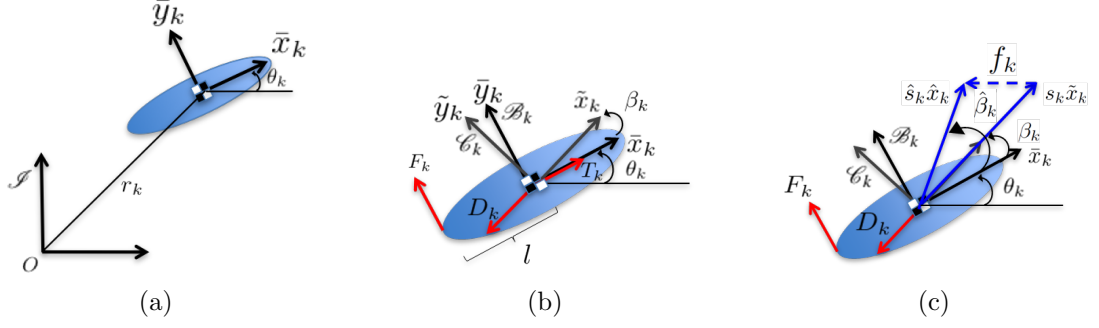


Figure 6.1: (a) Rigid-body model (b) Reference frames, no flow (c) Reference frames in flowfield f

is

$$\dot{r}_k = u_k \bar{x}_k + v_k \bar{y}_k. \quad (6.7)$$

The time-derivative of (6.7) with respect to inertial frame \mathcal{I} yields the rigid-body translational kinematics:

$$\ddot{r}_k = (\dot{u}_k - v_k \dot{\theta}_k) \bar{x}_k + (u_k \dot{\theta}_k + \dot{v}_k) \bar{y}_k. \quad (6.8)$$

We assume there are two control forces acting on the k th vehicle, as shown in Fig. 6.1b. The first is the thrust force T_k , which acts along the \bar{x}_k -axis. The steering control is F_k , which acts along the \bar{y}_k -axis a distance of l behind the center of mass. We also include a drag force $D_k = \frac{1}{2} \rho s_k^2 S C_D \triangleq h s_k^2$. (ρ is the density of the medium through which the vehicle is traveling; S is the vehicle reference area; and C_D is the appropriate drag coefficient.) The vehicle speed is $s_k = \sqrt{u_k^2 + v_k^2} \geq 0$.

We define a path frame for the k th vehicle as $\mathcal{C}_k = (k, \tilde{x}_k, \tilde{y}_k, \tilde{z}_k)$, where $\dot{r}_k = s_k \tilde{x}_k$ and $\tilde{z}_k = \bar{z}_k$. We denote the orientation of \mathcal{C}_k relative to \mathcal{B}_k as β_k . We assume the drag force acts in the $-\tilde{x}_k$ direction [28]. Using Newton's second law with mass

$m_k = m_0$ we have

$$(T_k - D_k \cos \beta_k) \bar{x}_k + (F_k - D_k \sin \beta_k) \bar{y}_k = m_0(\dot{u}_k - v_k \dot{\theta}_k) \bar{x}_k + m_0(u_k \dot{\theta}_k + \dot{v}_k) \bar{y}_k. \quad (6.9)$$

Collecting the \bar{x}_k terms, we have

$$T_k - D_k \cos \beta_k = m_0(\dot{u}_k - v_k \dot{\theta}_k). \quad (6.10)$$

We are able to obtain a dynamic expression for the forward speed u_k by solving (6.10) for \dot{u}_k :

$$\dot{u}_k = -\frac{1}{m_0} D_k \cos \beta_k + \frac{1}{m_0} T_k + v_k \dot{\theta}_k. \quad (6.11)$$

Following the same procedure for the terms in the \bar{y}_k -direction, we have

$$\dot{v}_k = -\frac{1}{m_0} D_k \sin \beta_k + \frac{1}{m_0} F_k - u_k \dot{\theta}_k. \quad (6.12)$$

In order to design the rotational dynamics, let M_k be the sum of the moments acting on the k th vehicle. Assuming there is no moment due to drag (i.e, the drag acts through the vehicle's center of mass), we have

$$M_k = (-l \bar{x}_k) \times (F_k \bar{y}_k). \quad (6.13)$$

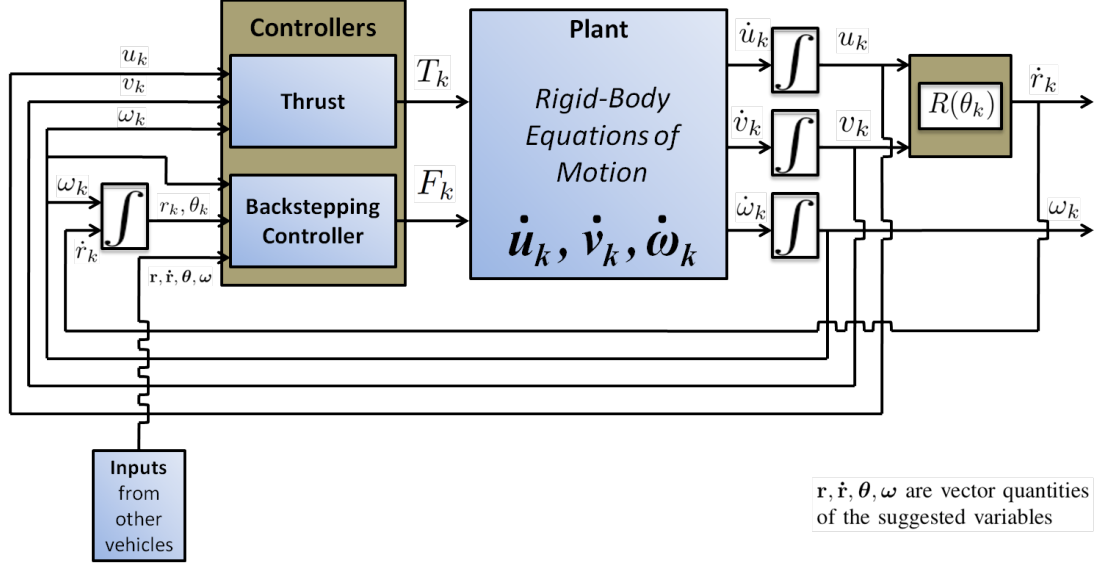


Figure 6.2: Block diagram for the rigid-body model.

The rotational dynamics are

$$I_k \ddot{\theta}_k = -l F_k, \quad (6.14)$$

where $I_k = I_0$ is the moment of inertia about the k th vehicle's center of mass. The equations of motion are

$$\begin{aligned} \dot{r}_k &= u_k \bar{x}_k + v_k \bar{y}_k = s_k \tilde{x}_k \\ \dot{u}_k &= -\frac{1}{m_0} D_k \cos \beta_k + \frac{1}{m_0} T_k + v_k \omega_k \\ \dot{v}_k &= -\frac{1}{m_0} D_k \sin \beta_k + \frac{1}{m_0} F_k - u_k \omega_k \\ \dot{\omega}_k &= -\frac{l}{I_0} F_k, \end{aligned} \quad (6.15)$$

where $\omega_k = \dot{\theta}_k$, $D_k = h s_k^2$, and $\beta_k = \arctan(v_k/u_k)$. T_k and F_k are the control forces.

In the following chapter we design T_k and F_k to be state-feedback controllers.

Chapter 7

Control of Planar Rigid-Body Dynamics

7.1 Parallel Formation Control

In this section we design a decentralized feedback control to drive a collection of planar rigid bodies described by (6.15) in the same direction at the same speed (i.e., in a parallel formation). In order to ensure that the steady-state forward speed of each vehicle is $u_k = u_0$, we use feedback linearization [16]. Choosing

$$T_k = m_0 \left(\frac{1}{m_0} D_k \cos \beta_k - v_k \omega_k + K_f (u_0 - u_k) \right), \quad (7.1)$$

where $K_f > 0$, yields the following closed-loop dynamics

$$\dot{u}_k = K_f (u_0 - u_k). \quad (7.2)$$

The dynamics (7.2) ensure u_k exponentially converges to u_0 .

Motivated by the backstepping procedure described in Chapters 3 and 4, we choose

$$F_k = -\frac{I_0}{I} a_k, \quad (7.3)$$

with a_k given by (3.7).

Theorem 6. *Consider the rigid body model (6.15) with thrust control (7.1) and*

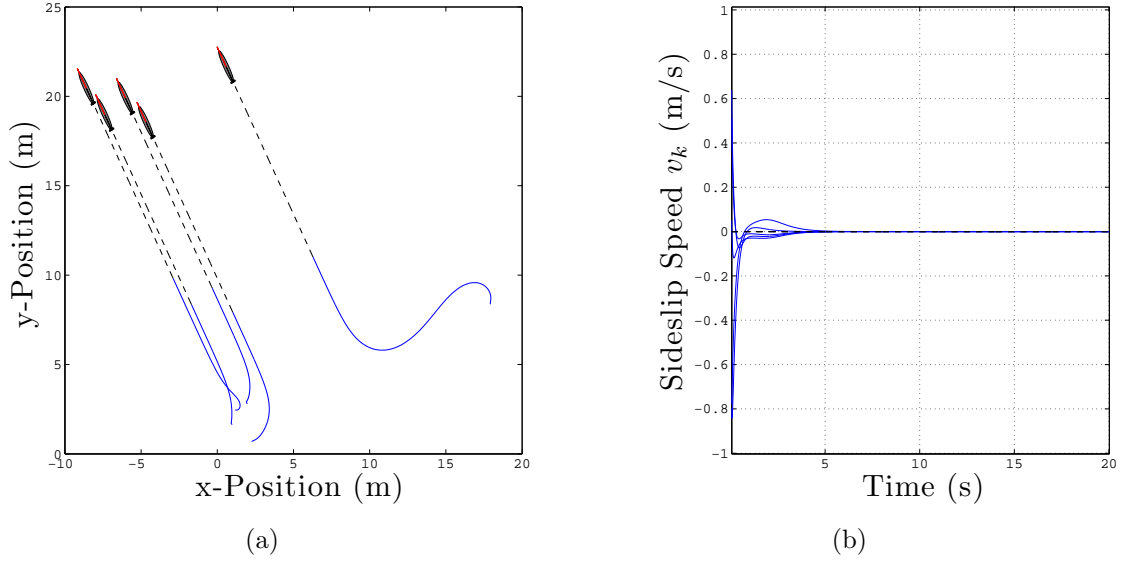


Figure 7.1: (a) Rigid-body parallel motion in the plane. (b) Velocity component of parallel motion. Randomly-generated initial conditions.

steering control (7.3), where a_k is given by (3.7). Under these controllers, the set of parallel formations, where $\beta_k = 0$ and $u_k = u_0$ for all k , and $\theta_k = \theta_j$ for all pairs j and k , is asymptotically stable.

Proof. In order to analyze the closed-loop system, we propose the following candidate Lyapunov function

$$U_{par}(\mathbf{u}, \mathbf{v}, \boldsymbol{\theta}, \mathbf{z}) = V_c + \frac{1}{2} \sum_{k=1}^N [(u_0 - u_k)^2 + v_k^2], \quad (7.4)$$

where $\mathbf{u} = [u_1, \dots, u_N]^T$, $\mathbf{v} = [v_1, \dots, v_N]^T$, $\mathbf{z} = [z_1, \dots, z_N]^T$, and where V_c is given by (3.4) with phase potential (3.2). Taking the time-derivative of U_{par} along solutions of (6.15) gives

$$\dot{U}_{par} = \dot{V}_c + \sum_{k=1}^N [-(u_0 - u_k)\dot{u}_k + v_k\dot{v}_k]. \quad (7.5)$$

Observe that $\dot{V}_c \leq 0$ under the steering control (3.7) and $a_k = a_k(\boldsymbol{\theta})$ is independent of the states u_k and v_k . Using (6.15) we obtain

$$\begin{aligned} \dot{U}_{par} &= \sum_{k=1}^N \left[\frac{K}{N} \langle p_\theta, i e^{i\theta_k} \rangle^2 - \kappa z_k^2 - K_f (u_0 - u_k)^2 \right] \\ &\quad + \sum_{k=1}^N \left[-\frac{1}{m_k} v_k D_k \sin \beta_k + \frac{1}{m_0} v_k F_k - v_k u_k \omega_k \right]. \end{aligned}$$

Recall that the drag is $D_k = h s_k^2 \geq 0$, where $h = \frac{1}{2} \rho S C_D$. Furthermore, $\sin \beta_k = v_k / s_k$, and $s_k \geq 0$. Consequently, $-v_k D_k \sin \beta_k = -h s_k v_k^2 \leq 0$.

According to the invariance principle, solutions converge to the largest invariant set Λ in which $\dot{V}_c = 0$, where Λ is given by (3.8). In Λ , $\omega_k \equiv 0$ because $z_k \equiv 0$ and $\phi_k \equiv 0$. Note that $\omega_k \equiv 0$ only if $\dot{\omega}_k = 0$ in Λ . Thus $F_k \equiv 0$ in Λ because $\dot{\omega}_k = a_k = -\frac{I_0}{I} F_k$. In Λ ,

$$\dot{U}_{par} = \sum_{k=1}^N \left[-K_f (u_0 - u_k)^2 - \frac{h}{m_0} s_k v_k^2 \right] \leq 0. \quad (7.6)$$

Application of the invariance principle in Λ shows that solutions starting in Λ converge to the largest set $M \subset \Lambda$ in which $\dot{U}_{par} = 0$. In M , $u_0 - u_k \equiv 0$ and $s_k v_k^2 \equiv 0$ which implies $u_k = u_0$ and $v_k = 0$. As a result, $\beta_k \equiv 0$ and M contains the set of parallel formations. The remainder of the proof follows from [33, Theorem 1]. \square

Theorem 6 is illustrated in Fig. 7.1a using $N = 5$, $K = -1$, $\kappa = 5$, and $u_0 = 1$. Note that the steady-state sideslip speed v_k is zero for parallel formations, but not for circular formations, as shown next. This leads to a non-zero crab angle β_k .

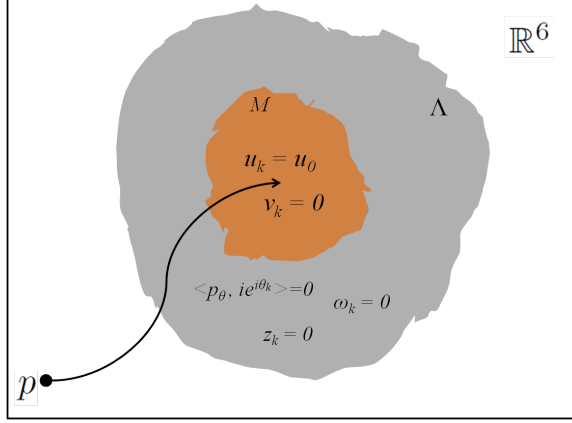


Figure 7.2: Illustration of the condition $\dot{U}_{par} = 0$. p is the initialization point in \mathbb{R}^6 .

7.2 Circular Formation Control

To stabilize circular formations, we use the thrust control (7.1). However, instead of using the steering control (7.3) with a_k given by (3.14), we now consider an alternative backstepping control that takes into account the observation that the steady-state crab angle β_k is not zero during a constant turn.

To find the steady-state crab angle and the corresponding steady-state speed, we differentiate $\tan \beta_k = v_k/u_k$ with respect to time and solve for $\dot{\beta}_k$ with $u_k = u_0 \neq 0$ to obtain

$$\dot{\beta}_k = \frac{\cos^2 \beta_k}{u_0} \left(-\frac{1}{m_0} D_k \sin \beta_k + \frac{1}{m_0} F_k - u_0 \omega_k \right). \quad (7.7)$$

For circular motion with constant speed $s_k = s_0$ and turning rate $\omega_k = \omega_0 s_0$, $F_k = \dot{\omega}_k = 0$, which implies

$$\dot{\beta}_k = \frac{\cos^2 \beta_k}{u_0} \left(-\frac{1}{m_0} D_k \sin \beta_k - u_0 \omega_0 s_0 \right). \quad (7.8)$$

The equilibrium points of (7.8) are $\beta_k = \beta_0$, where

$$\beta_0 = \pm\pi/2 \quad \text{and} \quad \beta_0 = \arcsin\left(-\frac{m_0 u_0 \omega_0}{h s_0}\right) \quad (7.9)$$

and we used $D_k = h s_0^2$ in equilibrium.

The equilibrium points $\beta_0 = \pm\pi/2$ are not possible for $u_k = u_0 \neq 0$ since $\cos \beta_0 = u_0/s_0 \neq 0$. For the second set of equilibrium points, s_0 and $v_0 = s_0 \sin \beta_0 = m_0 u_0 \omega_0/h$ are constant. To find s_0 , we solve $s_0^2 = u_0^2 + v_0^2$, obtaining

$$s_0 = \left(\frac{u_0^2 + \sqrt{u_0^4 + 4(m_0 u_0 \omega_0/h)^2}}{2} \right)^{1/2}. \quad (7.10)$$

One can show by linearization that the second set of equilibrium points for β_k are stable.

In light of this analysis, we modify the backstepping control (3.14) to allow for the vehicle speed $s_0 \neq 1$. The first step is to recognize that, along solutions to (6.15), the time derivative of the circle center $c_k = r_k + i\omega_0^{-1}e^{i(\theta_k + \beta_k)}$ becomes $\dot{c}_k = (s_k - \omega_0^{-1}\dot{\psi}_k)e^{i\psi_k}$, where $\psi_k = \theta_k + \beta_k$. As a result, the desired ω_k dynamics (3.9) become

$$\phi_k(\mathbf{r}, \mathbf{u}, \mathbf{v}, \boldsymbol{\psi}) = \omega_0(s_k + K\langle P_k \mathbf{c}, e^{i\psi_k} \rangle) - \dot{\beta}_k, \quad K > 0, \quad (7.11)$$

where $\boldsymbol{\psi} = [\psi_1, \dots, \psi_N]^T$. The backstepping control $\dot{\omega}_k = a_k$ that asymptotically

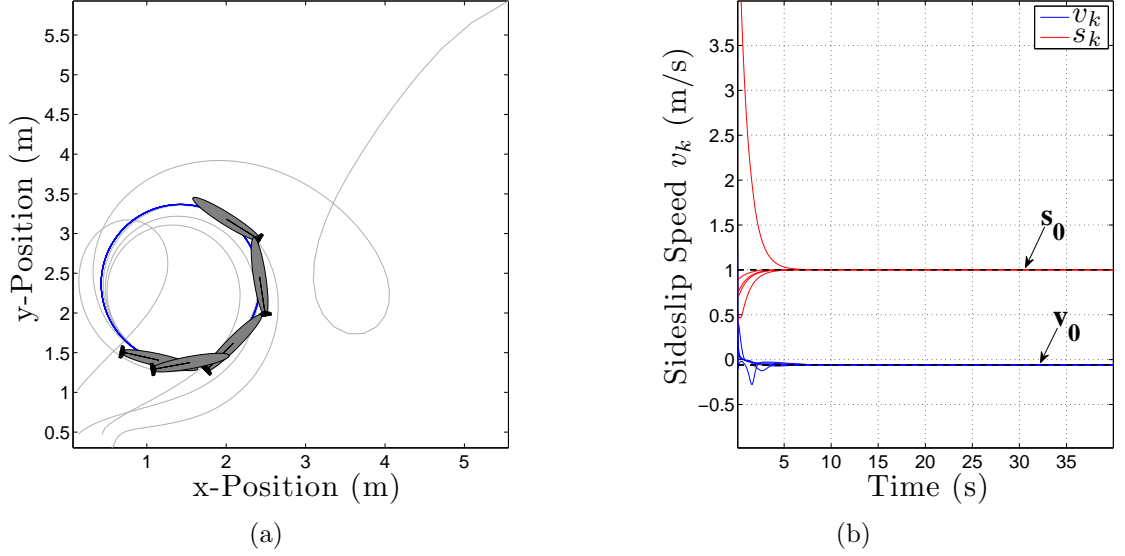


Figure 7.3: (a) Rigid-body circular motion in the plane. (b) Velocity component of circular motion with time. Randomly-generated initial conditions.

stabilizes $\omega_k = \phi_k(\mathbf{r}, \mathbf{u}, \mathbf{v}, \psi)$ is

$$\begin{aligned}
a_k &= -\kappa(\omega_k - \phi_k(\mathbf{r}, \mathbf{u}, \mathbf{v}, \psi)) + \omega_0 K \dot{\psi}_k \langle \tilde{r}_k, i e^{i\psi_k} \rangle - \ddot{\beta}_k \\
&\quad + K \left(\omega_0 s_k - \frac{1}{N} \sum_{j=1}^N \left[\langle e^{i\psi_j}, e^{i\psi_k} \rangle (\omega_0 s_j - (\dot{\psi}_j - \dot{\psi}_k)) \right] \right) \\
&\quad \omega_0 \dot{s}_k + \omega_0^{-1} \left(\langle \tilde{r}_k, e^{i\psi_k} \rangle - \omega_0^{-1} \frac{1}{N} \sum_{j=1}^N \langle i e^{i\psi_j}, e^{i\psi_k} \rangle \right),
\end{aligned} \tag{7.12}$$

where $\tilde{r}_k = r_k - \frac{1}{N} \sum_{j=1}^N r_j$, $K > 0$, and $\kappa > 0$. In practice, we omit the \dot{s}_k , $\dot{\beta}_k$, and $\ddot{\beta}_k$ terms from the control because they converge to zero in steady-state (since s_k converges to s_0 and β_k converges to β_0). We have the following result.

Theorem 7. *Consider the rigid body model (6.15) with thrust control (7.1) and steering control (7.3), where a_k is given by (7.12). Under these controllers, the set of circular formations with radius $1/|\omega_0|$ and direction of rotation determined by the sign of ω_0 is asymptotically stable. In this set, $u_k = u_0$ and $v_k = v_0 = m_0 u_0 \omega_0 / h$ for*

all k , and $c_j = c_k$ for all pairs j and k .

Proof. To determine if the chosen controllers for T_k and F_k establish the desired closed loop behavior, we begin by defining a Lyapunov function for circular formations as

$$U_{circ}(\mathbf{r}, \mathbf{u}, \mathbf{v}, \boldsymbol{\psi}, \mathbf{z}) = V_c + \frac{1}{2} \sum_{k=1}^N [(u_0 - u_k)^2 + (v_0 - v_k)^2], \quad (7.13)$$

where V_c is given by (3.13) with circle center $c_k = r_k + i\omega_0^{-1}e^{i\psi_k}$. Taking the time-derivative along solutions of (6.15) gives

$$\begin{aligned} \dot{U}_{circ} &= \sum_{k=1}^N [-K \langle P_k \mathbf{c}, e^{i\psi_k} \rangle^2 - \kappa z_k^2] \\ &+ \sum_{k=1}^N \left[-(u_0 - u_k) \left(-\frac{1}{m_0} D_k \cos \beta_k + \frac{1}{m_0} T_k + v_k \omega_k \right) \right] \\ &+ \sum_{k=1}^N \left[(v_0 - v_k) \left(\frac{1}{m_0} D_k \sin \beta_k - \frac{1}{m_0} F_k + u_k \omega_k \right) \right]. \end{aligned} \quad (7.14)$$

Choosing T_k to be the stabilizing control (7.1) ensures that u_k converges to u_0 according to the closed-loop dynamics (7.2). Furthermore, $\dot{V}_c \leq 0$ along solutions of (6.15). Therefore, solutions converge to the largest invariant set Λ in which $u_k - u_0 \equiv 0$ and $\dot{V}_c \equiv 0$, i.e.,

$$\Lambda = \{ \langle P_k \mathbf{c}, i e^{i\psi_k} \rangle \equiv 0, z_k \equiv 0, u_k \equiv u_0, \forall k \}. \quad (7.15)$$

In Λ , $\omega_k \equiv \omega_0 s_0$ and $F_k \equiv 0$, which implies that $s_0 \equiv [u_0^2 + (-m_0 u_0 \omega_0 / h)^2]^{1/2}$ and

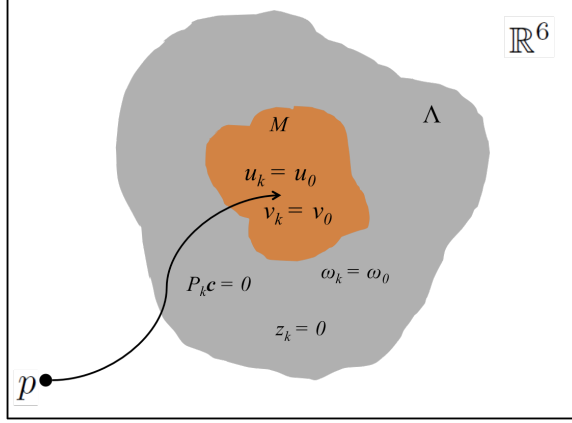


Figure 7.4: Illustration of the condition $\dot{U}_{circ} = 0$. p is the initialization point in \mathbb{R}^6 .

$v_0 = -m_0 u_0 \omega_0 / h$. For solutions starting in Λ , we have

$$\begin{aligned} \dot{U}_{circ} &= \sum_{k=1}^N (v_0 - v_k) (h s_0 v_k / m_0 + u_k \omega_0 s_0) \\ &= \sum_{k=1}^N -\frac{h s_0}{m_0} (v_0 - v_k)^2 \leq 0. \end{aligned} \tag{7.16}$$

Application of the invariance principle in Λ shows that solutions starting in Λ converge to the largest set $M \subset \Lambda$ in which $\dot{U}_{circ} = 0$. M contains the set of circular formations with $u_k \equiv u_0$ and $v_k \equiv v_0$. \square

Theorem 7 is illustrated in Fig. 7.3a with $N = 5$, $K = 1$, $\kappa = 5$, $\omega_0 = 1$, and $u_0 = 1$. Since the sideslip speed v_k converges to v_0 (shown in Fig. 7.3b) and u_k converges to u_0 , all N vehicles travel around circular trajectories of identical radius. Though the centers are co-located, Theorem 7 does not specify the position of the steady-state formation center. When we wish to prescribe the center of the circular formation, rather than allow it to be arbitrary, we introduce a reference center as described next.

Let c_0 denote the location of the desired formation center. We also define the

constant $a_{k,0}$, where $a_{k,0} = 1$ if the k th vehicle is informed of the center location c_0 , and $a_{k,0} = 0$ if the vehicle is uninformed. In practice, only a single vehicle needs to be informed of c_0 [29]. Noting that $\psi_k = \theta_k + \beta_k$, the controller for a first-order model is [29]

$$\dot{\phi}_k = \omega_0 \left[s_k + K(\langle e^{i\psi_k}, P_k \mathbf{c} \rangle + a_{k,0} \langle e^{i\psi_k}, c_k - c_0 \rangle) \right] - \dot{\beta}_k. \quad (7.17)$$

To derive this controller, we use the composite Lyapunov function [27]

$$V = \frac{1}{2} \langle \mathbf{c}, P \mathbf{c} \rangle + \frac{1}{2} \sum_{k=1}^N a_{k,0} |c_k - c_0|^2. \quad (7.18)$$

The first term of this Lyapunov function ensures that all circular centers are the same. The second term imposes the additional condition that all circular centers reach the desired center location c_0 . Taking the time-derivative of (7.18) we have

$$\dot{V} = \sum_{k=1}^N \left(\langle e^{i\psi_k}, P_k \mathbf{c} \rangle + a_{k,0} \langle e^{i\psi_k}, c_k - c_0 \rangle \right) (s_k - \omega_0^{-1}(\dot{\theta}_k + \dot{\beta}_k)). \quad (7.19)$$

Substituting (7.17) for $\dot{\theta}_k$, we have

$$\dot{V} = -K \sum_{k=1}^N \left(\langle e^{i\psi_k}, P_k \mathbf{c} \rangle + a_{k,0} \langle e^{i\psi_k}, c_k - c_0 \rangle \right)^2 \leq 0. \quad (7.20)$$

To extend these results to the second-order model, we use the Lyapunov function

$$V_c = \frac{1}{2} \langle \mathbf{c}, P \mathbf{c} \rangle + \frac{1}{2} \sum_{k=1}^N [a_{k,0} |c_k - c_0|^2 + z_k^2]. \quad (7.21)$$

Taking the time-derivative gives

$$\dot{V}_c = \sum_{k=1}^N \left[\left(\langle e^{i\psi_k}, P_k \mathbf{c} \rangle + a_{k,0} \langle e^{i\psi_k}, c_k - c_0 \rangle \right) (s_k - \omega_0^{-1}(\dot{\theta}_k + \dot{\beta}_k)) + z_k \nu_k \right]. \quad (7.22)$$

Let $\dot{\theta}_k = \phi_k + z_k$, where ϕ_k is given by (7.17). Then we have

$$\begin{aligned} \dot{V}_c &= \sum_{k=1}^N \left[-K \left(\langle e^{i\psi_k}, P_k \mathbf{c} \rangle + a_{k,0} \langle e^{i\psi_k}, c_k - c_0 \rangle \right)^2 \right] \\ &\quad + \sum_{k=1}^N \left[-\omega_0^{-1} \left(\langle e^{i\psi_k}, P_k \mathbf{c} \rangle + a_{k,0} \langle e^{i\psi_k}, c_k - c_0 \rangle \right) z_k + z_k \nu_k \right]. \end{aligned} \quad (7.23)$$

Choosing $\nu_k = \omega_0^{-1} \left(\langle e^{i\psi_k}, P_k \mathbf{c} \rangle + a_{k,0} \langle e^{i\psi_k}, c_k - c_0 \rangle \right) - \kappa z_k$ implies that

$$\dot{V}_c = \sum_{k=1}^N \left[-K \left(\langle e^{i\psi_k}, P_k \mathbf{c} \rangle + a_{k,0} \langle e^{i\psi_k}, c_k - c_0 \rangle \right)^2 - \kappa z_k^2 \right]. \quad (7.24)$$

Using the transformation $a_k = \nu_k + \dot{\phi}_k$, along with the transformation $z_k = \omega_k - \phi_k$, the second-order controller is

$$\begin{aligned} a_k &= -\kappa(\dot{\psi}_k - \phi_k) + \omega_0 K \dot{\psi}_k \langle \tilde{r}_k, i e^{i\psi_k} \rangle + \omega_0 \dot{s}_k \\ &\quad + K \left(\omega_0 s_k - \frac{1}{N} \sum_{j=1}^N \left[\langle e^{i\psi_j}, e^{i\psi_k} \rangle (\omega_0 s_j - (\dot{\psi}_j - \dot{\psi}_k)) \right] \right) \\ &\quad + \omega_0^{-1} \left(\langle \tilde{r}_k, e^{i\psi_k} \rangle - \omega_0^{-1} \frac{1}{N} \sum_{j=1}^N \langle i e^{i\psi_j}, e^{i\psi_k} \rangle \right) \\ &\quad + \omega_0^{-1} a_{k,0} \langle i e^{i\psi_k}, c_k - c_0 \rangle \dot{\psi}_k + \omega_0^{-1} a_{k,0} (s_k - \omega_0^{-1} \dot{\psi}_k) - \ddot{\beta}_k. \end{aligned} \quad (7.25)$$

We have the following result.

Corollary 1. *Consider the rigid body model (6.15) with thrust control (7.1) and steering control (7.3), where a_k is given by (7.25). Under these controllers, the set*

of circular formations with radius $1/|\omega_0|$ and direction of rotation determined by the sign of ω_0 is asymptotically stable. In this set, $u_k = u_0$ and $v_k = v_0 = -m_0 u_0 \omega_0 / h$ for all k , and $c_j = c_k$ for all pairs j and k . The steady-state circle center is c_0 as long as at least one $a_{k,0} \in \{0, 1\}$, where $k = 1, \dots, N$, is equal to 1.

Chapter 8

Control of Planar Rigid-Body Dynamics in a Uniform Flowfield

The previous chapter provided formation controls in the absence of a flowfield. We now analyze the performance of a group of vehicles when a known, time-invariant, uniform flowfield is considered. In the presence of a flowfield we assume the velocity of the k th vehicle is the vector sum of the flowfield and the vehicle velocity relative to the flow (see Fig. 1.1c). Designating the crab angle in a flowfield as $\hat{\beta}_k$, we have

$$\dot{r}_k = u_k \bar{x}_k + v_k \bar{y}_k + f_k \triangleq \hat{s}_k e^{i\gamma_k}, \quad (8.1)$$

where $\gamma_k = \arg\{\dot{r}_k\} = \theta_k + \hat{\beta}_k$ and $\hat{s}_k = |\dot{r}_k|$. The speed is

$$\hat{s}_k = \sqrt{\hat{u}_k^2 + \hat{v}_k^2}, \quad (8.2)$$

where

$$\hat{u}_k = u_k + \langle f_k, \bar{x}_k \rangle \quad (8.3)$$

and

$$\hat{v}_k = v_k + \langle f_k, \bar{y}_k \rangle. \quad (8.4)$$

Note that the drag force, $D_k = hs_k^2$, in Fig. 6.1c is oriented opposite to the vehicle velocity relative to the flow.

To find the equations of motion, we take the time-derivative of (8.3) and (8.4)

to obtain

$$\begin{aligned}\dot{\hat{u}}_k &= \dot{u}_k + \langle f_k, \dot{\theta}_k \bar{y}_k \rangle \\ &= -\frac{1}{m_0} D_k \cos \beta_k + \frac{1}{m_0} T_k + \hat{v}_k \omega_k,\end{aligned}\tag{8.5}$$

and

$$\begin{aligned}\dot{\hat{v}}_k &= \dot{v}_k + \langle f_k, -\dot{\theta}_k \bar{x}_k \rangle \\ &= -\frac{1}{m_0} D_k \sin \beta_k + \frac{1}{m_0} F_k - \hat{u}_k \omega_k,\end{aligned}\tag{8.6}$$

respectively. We compute s_k by rewriting (8.2) as

$$\hat{s}_k^2 = s_k^2 + 2(u_k \langle f_k, \bar{x}_k \rangle + v_k \langle f_k, \bar{y}_k \rangle) + \langle f_k, \bar{x}_k \rangle^2 + \langle f_k, \bar{y}_k \rangle^2\tag{8.7}$$

and solving for s_k in terms of \hat{u}_k and \hat{v}_k to obtain

$$s_k = \left(\hat{s}_k^2 - 2\hat{u}_k \langle f_k, \bar{x}_k \rangle - 2\hat{v}_k \langle f_k, \bar{y}_k \rangle + \langle f_k, \bar{x}_k \rangle^2 + \langle f_k, \bar{y}_k \rangle^2 \right)^{1/2}.\tag{8.8}$$

The equations of motion are

$$\begin{aligned}\dot{r}_k &= u_k \bar{x}_k + v_k \bar{y}_k + f_k = s_k \tilde{x}_k + f_k \triangleq \hat{s}_k \hat{x}_k \\ \dot{\hat{u}}_k &= -\frac{1}{m_0} D_k \cos \beta_k + \frac{1}{m_0} T_k + \hat{v}_k \omega_k \\ \dot{\hat{v}}_k &= -\frac{1}{m_0} D_k \sin \beta_k + \frac{1}{m_0} F_k - \hat{u}_k \omega_k \\ \dot{\omega}_k &= -\frac{l}{I_0} F_k.\end{aligned}\tag{8.9}$$

Note, we will make use of a new path frame $\mathcal{F}_k = (k, \hat{x}_k, \hat{y}_k, \hat{z}_k)$, where \hat{x}_k is the inertial direction of motion, $\hat{z}_k = \bar{z}_k$, and $\hat{y}_k = \hat{z}_k \times \hat{x}_k$.

8.1 Parallel Formation Control

In this section we design a decentralized feedback control to drive a collection of planar rigid bodies in the same inertial direction at the same speed relative to the flowfield. To ensure that the forward speed relative to the flow converges to u_0 we use

$$T_k = m_0 \left(\frac{1}{m_0} D_k \cos \beta_k - v_k \omega_k + K_f (u_0 - u_k) \right). \quad (8.10)$$

Under this controller, $\dot{u}_k = K_f (u_0 - u_k) + \omega_k \langle f, \bar{y}_k \rangle$ and $\dot{v}_k = K_f (u_0 - u_k)$, which ensures u_k converges to u_0 . We stabilize the orientation and turning rate of the k th vehicle using

$$F_k = -\frac{I_0}{l} \lambda_k, \quad (8.11)$$

with λ_k given by (4.3).

Next we determine the steady-state crab angles $\hat{\beta}_0$ and β_0 . To find $\hat{\beta}_0$, we take the time-derivative of $\tan \hat{\beta}_k = \hat{v}_k / \hat{u}_k$ to obtain

$$\sec^2 \hat{\beta}_k \dot{\hat{\beta}}_k = \frac{\hat{u}_k \dot{\hat{v}}_k - \hat{v}_k \dot{\hat{u}}_k}{\hat{u}_k^2}. \quad (8.12)$$

Solving for $\dot{\hat{\beta}}_k$ and plugging in the appropriate expressions from (8.9) gives

$$\begin{aligned} \dot{\hat{\beta}}_k &= \frac{\cos^2 \hat{\beta}_k}{\hat{u}_k^2} \left[\hat{u}_k \left(-\frac{1}{m_0} D_k \sin \beta_k + \frac{1}{m_0} F_k - \hat{u}_k \omega_k \right) \right] \\ &\quad - \frac{\cos^2 \hat{\beta}_k}{\hat{u}_k^2} \left[\hat{v}_k \left(-\frac{1}{m_0} D_k \cos \beta_k + \frac{1}{m_0} T_k + \hat{v}_k \omega_k \right) \right]. \end{aligned} \quad (8.13)$$

The choice of T_k in (8.10) drives u_k to u_0 , which means that \dot{u}_k converges to $\dot{u}_k =$

$\omega_k \langle f, \bar{y}_k \rangle$. In steady-state parallel motion, where $F_k = 0$, we have

$$\dot{\hat{\beta}}_k = \frac{\cos^2 \hat{\beta}_k}{\hat{u}_k^2} \left[\hat{u}_k \left(-\frac{1}{m_0} D_k \sin \beta_k - \hat{u}_k \omega_k \right) - \hat{v}_k \omega_k \langle f, \bar{y}_k \rangle \right]. \quad (8.14)$$

To satisfy the equilibrium condition, $\dot{\hat{\beta}}_k = 0$, we identify $\hat{\beta}_0 = \pm\pi/2$ and

$$\beta_0 = \arcsin \left[-\left(\frac{\hat{v}_k \langle f, \bar{y}_k \rangle + \hat{u}_k}{\hat{u}_k} \right) \frac{m_0 \omega_k}{h s_k^2} \right]. \quad (8.15)$$

For parallel motion, $\omega_k = 0$, and as a result $\beta_0 = 0$, which implies that $v_0 = 0$ and $s_0 = u_0$. Recalling that

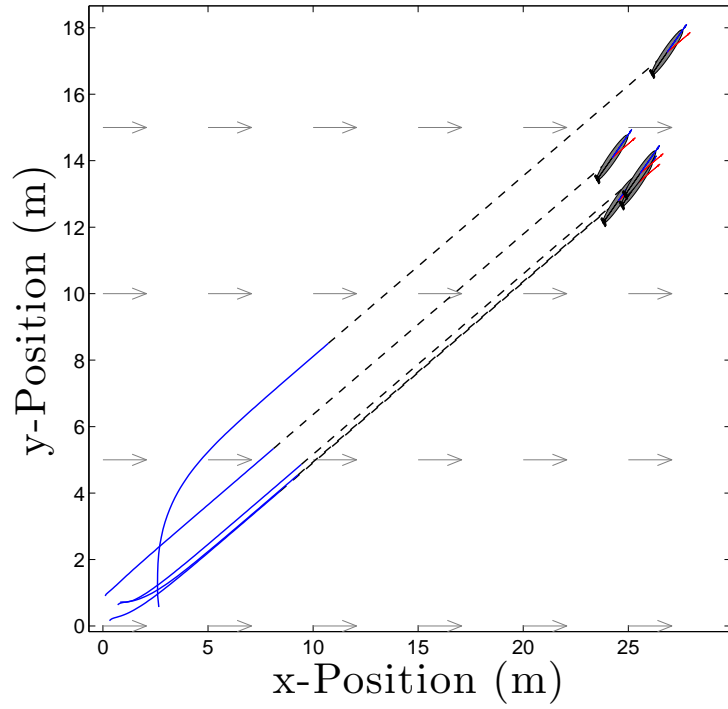
$$\hat{\beta}_k = \arctan \left(\frac{v_k + \langle f_k, \bar{y}_k \rangle}{u_k + \langle f_k, \bar{x}_k \rangle} \right) \quad (8.16)$$

and that \hat{s}_k can be expressed as (8.7), we have

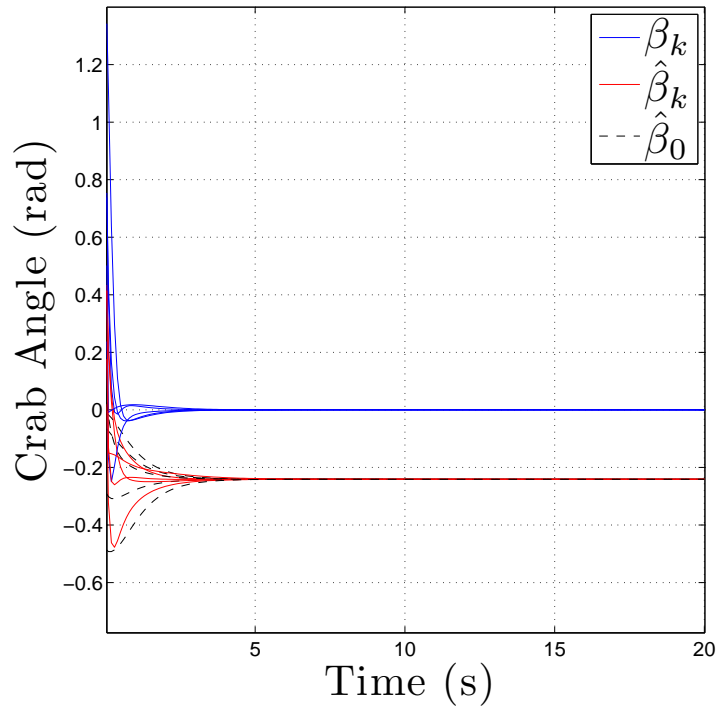
$$\begin{aligned} \hat{\beta}_0 &= \arctan \left(\frac{\langle f_k, \bar{y}_k \rangle}{u_0 + \langle f_k, \bar{x}_k \rangle} \right) \\ \hat{s}_0 &= \sqrt{s_0^2 + 2u_0 \langle f_k, \bar{x}_k \rangle + \langle f_k, \bar{x}_k \rangle^2 + \langle f_k, \bar{y}_k \rangle^2}. \end{aligned} \quad (8.17)$$

Theorem 8. *Consider the rigid body model (8.9) with thrust control (8.10) and steering control (8.11), where λ_k is given by (4.3). Under these controllers, the set of parallel formations where $\beta_k = 0$, $u_k = u_0$ for all k , and $\gamma_k = \gamma_j$ for all pairs j and k is asymptotically stable.*

Proof. In order to analyze the closed-loop system, we propose the following candi-



(a)



(b)

Figure 8.1: (a) Rigid body parallel motion in a flowfield. Blue arrows represent the direction of heading; red arrows represent the total velocity. (b) Crab angles β_k and $\hat{\beta}_k$ with time. Randomly initialized.

date Lyapunov function

$$U_{par}(\hat{\mathbf{u}}, \hat{\mathbf{v}}, \boldsymbol{\gamma}, \mathbf{z}) = V_c + \frac{1}{2} \sum_{k=1}^N [(\hat{u}_k - \langle f, \bar{x}_k \rangle - u_0)^2 + \hat{v}_k^2], \quad (8.18)$$

where $\hat{\mathbf{u}} = [\hat{u}_1, \dots, \hat{u}_N]$, $\hat{\mathbf{v}} = [\hat{v}_1, \dots, \hat{v}_N]$, and $\hat{\boldsymbol{\gamma}} = [\hat{\gamma}_1, \dots, \hat{\gamma}_N]$. V_c is given by (4.1) with phase potential $V(\boldsymbol{\gamma}) = \frac{1}{2}(1 - |p_\gamma|^2)$, and where $p_\gamma = \frac{1}{N} \sum_{j=1}^N e^{i\gamma_j}$. Taking the time-derivative along solutions of (8.9) gives

$$\dot{U}_{par} = \dot{V}_c + \sum_{k=1}^N \left[(\hat{u}_k - \langle f, \bar{x}_k \rangle - u_0) \left(-\frac{1}{m_0} D_k \cos \beta_k + \frac{1}{m_0} T_k + v_k \omega_k \right) + \hat{v}_k \dot{\hat{v}}_k \right]. \quad (8.19)$$

Observe that $\dot{V}_c \leq 0$ under the steering control (4.3) and that $a_k = a_k(\boldsymbol{\gamma})$ is independent of the states \hat{u}_k and \hat{v}_k . If we plug in for $\dot{\hat{u}}_k$ and $\dot{\hat{v}}_k$ using (8.9) with thrust control (8.10) we obtain

$$\begin{aligned} \dot{U}_{par} &= \sum_{k=1}^N \left[\frac{K}{N} \langle p_\gamma, i e^{i\gamma_k} \rangle^2 - \kappa z_k^2 - K_f (u_0 - u_k)^2 \right] \\ &\quad + \sum_{k=1}^N \left[-\frac{1}{m_0} \hat{v}_k D_k \sin \beta_k + \frac{1}{m_0} \hat{v}_k F_k - \hat{v}_k u_k \omega_k \right]. \end{aligned}$$

Recall the drag is $D_k = h s_k^2 \geq 0$, where $h = \frac{1}{2} \rho S C_D$. Additionally, $\sin \beta_k = v_k / s_k$, and $s_k \geq 0$. Consequently, $-\hat{v}_k D_k \sin \beta_k = -\hat{v}_k h s_k v_k$.

According to the invariance principle, solutions converge to the largest invariant set Λ in which $\dot{V}_c = 0$, where Λ is given by

$$\Lambda = \{ \langle p_\gamma, i e^{i\gamma_k} \rangle \equiv 0, z_k \equiv 0 \forall k \}. \quad (8.20)$$

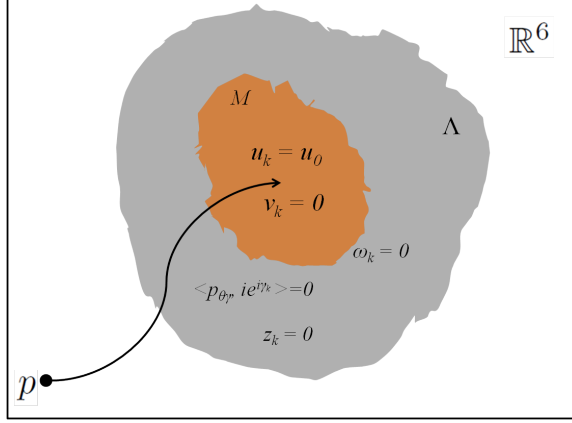


Figure 8.2: Illustration of the condition $\dot{U}_{par} = 0$ in a flowfield. p is the initialization point in \mathbb{R}^6 .

In Λ , $\omega_k \equiv 0$, because $z_k \equiv 0$ and $\phi_k \equiv 0$. Note that $\omega_k \equiv 0$ only if $\dot{\omega}_k = 0$ in Λ .

Thus $F_k \equiv 0$ in Λ because $\dot{\omega}_k = a_k = -\frac{I_k}{l} F_k$. In Λ ,

$$\dot{U}_{par} = \sum_{k=1}^N \left[-K_f(u_0 - u_k)^2 - \frac{1}{m_0} \hat{v}_k h s_k v_k - \hat{v}_k u_k \omega_k \right] \leq 0. \quad (8.21)$$

Application of the invariance principle in Λ shows that solutions starting in Λ converge to the largest set $M \subset \Lambda$ in which $\dot{U}_{par} = 0$. In M , $u_0 - u_k = 0$ and $-\frac{1}{m_0} \hat{v}_k h s_k v_k - \hat{v}_k u_k \omega_k \equiv 0$ which implies $v_k = -m_0 u_k \omega_k / h s_k$. As a result, $\beta_k = \arcsin(-m_0 u_k \omega_k / h s_k^2)$ and M contains the set of parallel formations in a flowfield. The remainder of the proof follows from [33, Theorem 1]. \square

Theorem 8 is illustrated in Fig. 8.1a with $N = 5$, $K = -1$, $\kappa = 5$, $u_0 = 1$, and $f_k = 0.5$. Since the turning rate converges to zero in Λ , $\beta_0 = 0$, as shown in Fig. 8.1b. The inertially-measured sideslip velocity \hat{v}_k is a function of the flowfield, which implies that for constant heading, $\hat{\beta}_k$ converges to a constant equal to $\hat{\beta}_0 = \arctan(\langle f_k, \bar{y}_k \rangle / (u_0 + \langle f_k, \bar{x}_k \rangle))$.

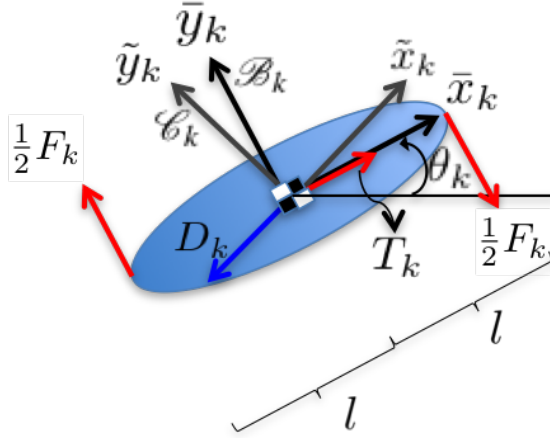


Figure 8.3: Diagram of the modified vehicle, with a moment couple realized by control surfaces at the tail and nose.

8.2 Circular Formation Control

When no flowfield was considered, we saw that achieving circular formations with performance comparable to the second-order vehicle model was feasible; this is primarily because the crab angle β_k converges to a constant for a constant turning rate ω_0 . When a flowfield is considered, the crab angle $\hat{\beta}_k$ depends on the yaw, θ_k , and is not constant for circular motion. As a result, the backstepping controller for circular formations in a flowfield is not feasible, because it is a function of $\hat{\beta}_k$ and $\ddot{\beta}_k$. These quantities are recursive functions of the steering force F_k that do not converge to zero, even if F_k does.

To solve this problem, we consider an alternate model of the vehicle dynamics. In the modified dynamics shown in Fig. 8.3, we replace the steering force with a moment couple. Half of the former steering force is applied in its original location and orientation at the rear of the vehicle; the other half is applied along the $-\bar{y}_k$ -direction a distance of $l\bar{x}_k$ forward of the center of mass. The equations of motion

become

$$\begin{aligned}
\dot{r}_k &= u_k \bar{x}_k + v_k \bar{y}_k + f_k = s_k \tilde{x}_k + f_k = \hat{s}_k \hat{x}_k \\
\dot{\hat{u}}_k &= -\frac{1}{m_0} D_k \cos \beta_k + \frac{1}{m_0} T_k + \hat{v}_k \omega_k \\
\dot{\hat{v}}_k &= -\frac{1}{m_0} D_k \sin \beta_k - \hat{u}_k \omega_k \\
\dot{\omega}_k &= -\frac{l}{I_k} F_k.
\end{aligned} \tag{8.22}$$

With these equations, $\dot{\hat{\beta}}_k$ is found by

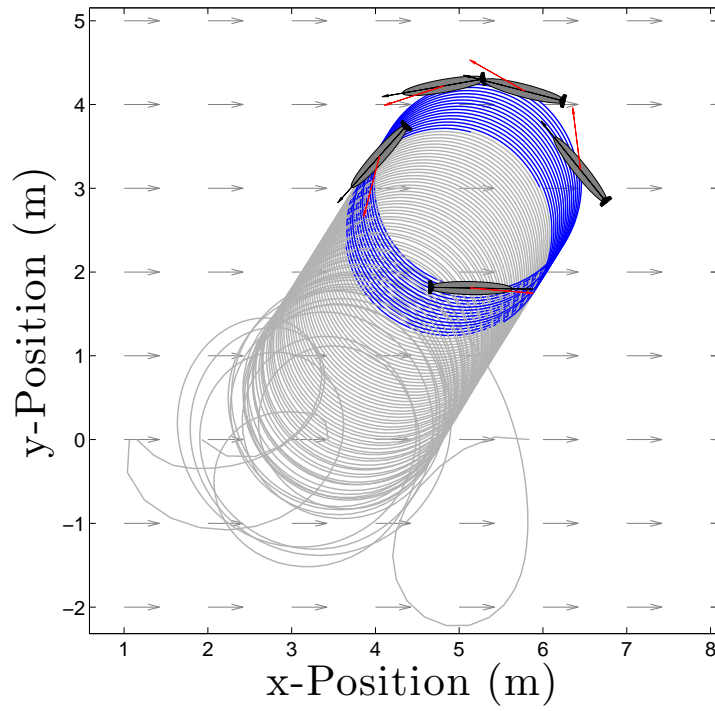
$$\dot{\hat{\beta}}_k = \frac{\cos^2 \hat{\beta}_k}{\hat{u}_k^2} \left(-\hat{v}_k \dot{\hat{u}}_k + \hat{u}_k \dot{\hat{v}}_k \right) = \frac{1}{\hat{s}_k} \left[\cos \hat{\beta}_k \dot{\hat{v}}_k - \sin \hat{\beta}_k \dot{\hat{u}}_k \right], \tag{8.23}$$

where $\dot{\hat{u}}_k$ and $\dot{\hat{v}}_k$ are fully-specified functions given by (8.22). However, $\ddot{\hat{\beta}}_k$ is still a recursive function of the control F_k . This precludes the implementation of the backstepping controller, even after modifying the rigid body model. Therefore, we propose to use the proportional-integral controller

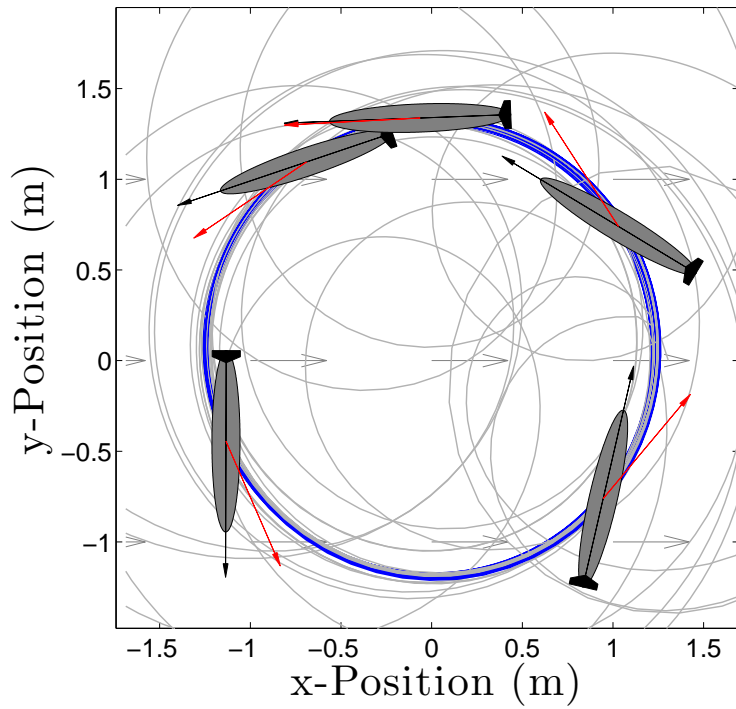
$$\dot{\omega}_k = K_P(\phi_k - \omega_k) + K_I \int (\phi_k - \omega_k) dt, \tag{8.24}$$

where ϕ_k is given by (7.17) with ψ replaced by γ and s replaced by \hat{s} . This controller only depends on $\dot{\hat{\beta}}_k$, (which is not a recursive function of the control F_k) and it drives ω_k to track ϕ_k . Even small tracking error $z_k = \phi_k - \omega_k$ has been observed to lead to drifting of the circle center. To resolve this issue, one can use the controller for circular formations with a prescribed center.

Proposition 1. *Consider the rigid body model (8.22) with thrust control (8.10) and steering control (8.11), where λ_k is given by (8.24). Under these controllers, the*



(a)



(b)

Figure 8.4: Circular motion in a flowfield (a) without a prescribed center and (b) with a prescribed center at $[0, 0]$. Black arrows show the direction of heading, red arrows indicate the total velocity. Randomly-generated initial conditions.

set of circular formations in a flowfield with radius $1/|\omega_0|$ and direction of rotation determined by the sign of ω_0 is asymptotically stable. In this set $u_k = u_0$ and $v_k = v_0 = s_0 \sin \beta_0$ for all k , and $c_j = c_k$ for all pairs j and k .

Proposition 1 is illustrated in Fig. 8.4b with $N = 5$, $K = 1$, $K_f = 1$, $K_P = 10$, $K_I = 15$, $\omega_0 = 0.8$, $u_0 = 1$, and $f_k = 0.5$. Fig. 8.5b shows that the inertially-measured crab angle $\hat{\beta}_k$ oscillates with time as a function of the vehicle's heading.

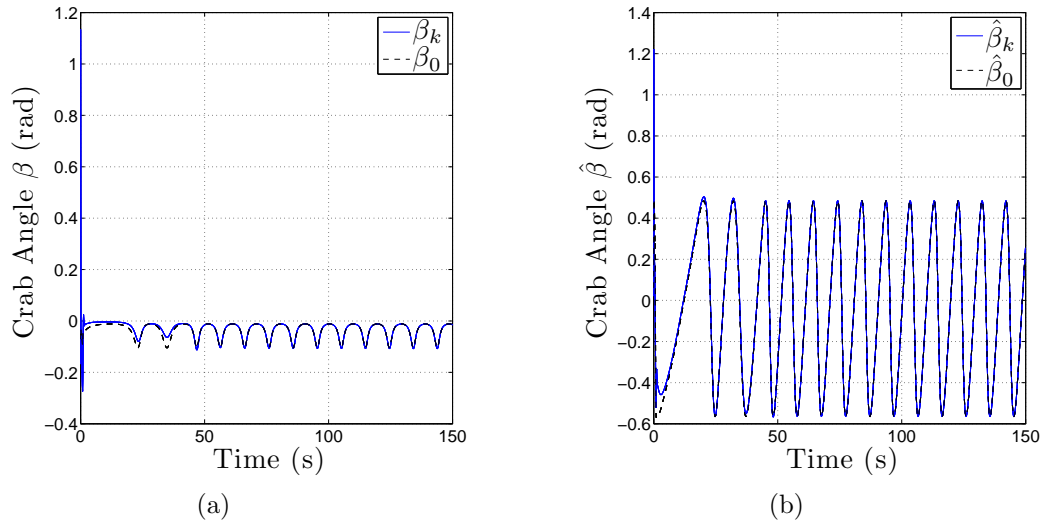


Figure 8.5: (a) Locally-measured crab angle.(b) Inertially-measured crab angle with time. Results are shown for only one vehicle.

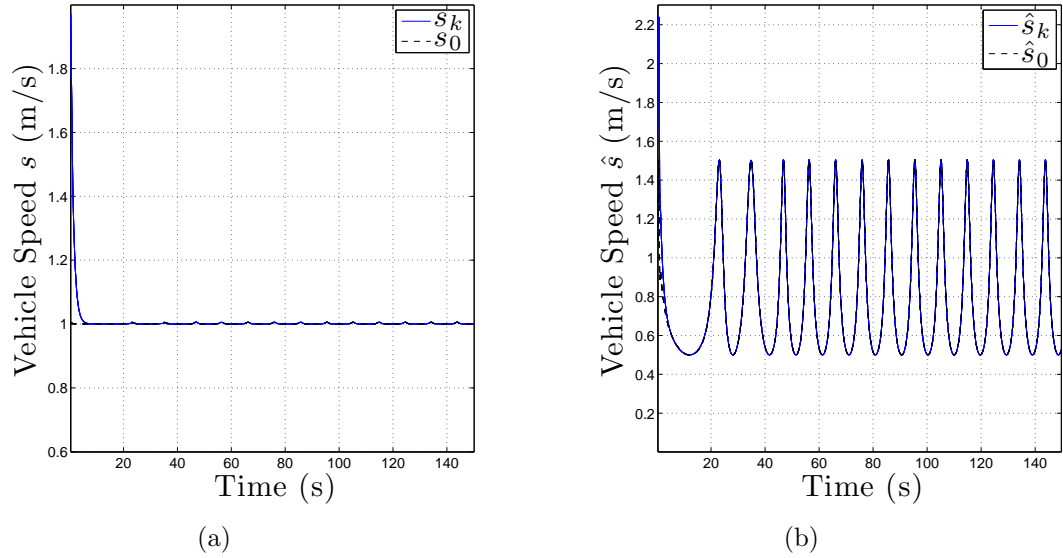


Figure 8.6: (a) Total speed s_k in the body frame. (b) Inertially-measured speed of the k th vehicle. Results are shown for only one vehicle.

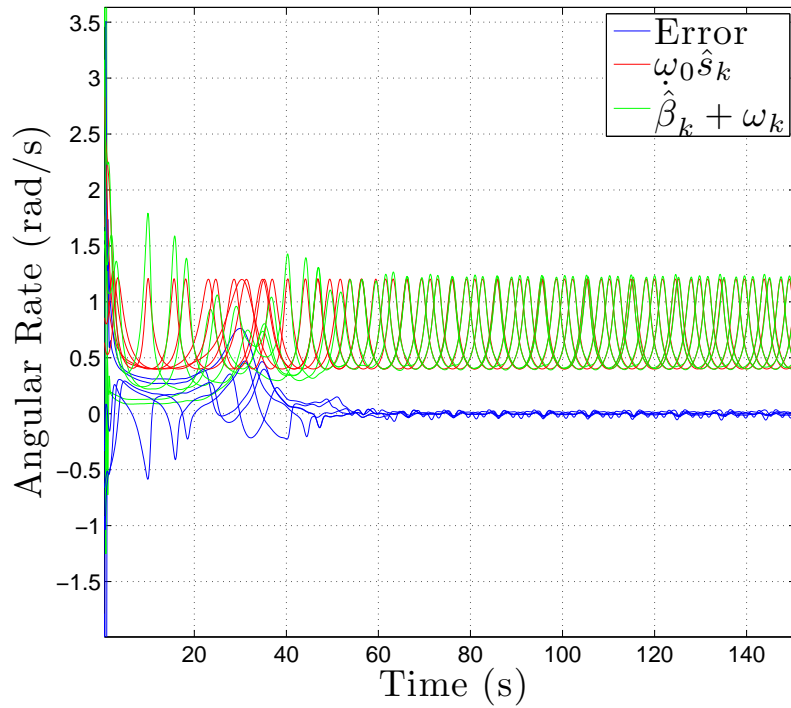


Figure 8.7: Steady-state error $\omega_0 \hat{s}_k - \dot{\beta}_k - \omega_k$ vs. time. Results are shown for all vehicles.

Chapter 9

Conclusion

The goal of this thesis is to provide a rigid body model for the collective motion of N autonomous vehicles. Existing first-order particle models enable N vehicles to achieve cooperative formation control. This thesis builds upon that foundation by first devising a backstepping control design for the stabilization of formations of N self-propelled particles with second-order rotational dynamics. Stabilization of the higher-ordered system relies on the assumed stability of the original system, as presented in [33] and [27]. In exploiting the Lyapunov functions used to prove the stability of formations with first-order rotational dynamics, composite Lyapunov functions, used to design controls to stabilize formations in the higher-ordered system, are constructed. The backstepping controller is more robust than a proportional controller in that, under the chosen Lyapunov function, backstepping allows us to eliminate the error dynamics whereas the proportional controller only guarantees convergence for a certain range of error.

Regardless of the controller chosen, there are certain requirements that each vehicle must meet. The first requirement is that each vehicle know the local flow-field. The second requirement is the result of extending the first-order models to include second-order dynamics; this introduces the new sensing requirement that each vehicle be able to measure its own angular velocity.

A rigid-body model has been devised for use with the second-order backstepping-derived steering controllers for the cooperative control of multiple vehicles. Rather than being treated as point masses, each vehicle has been represented as a planar rigid-body with second-order translational and rotational dynamics. In order to have closed-loop behavior in which the swarm of vehicles achieves parallel and circular formations, theoretically justified thrust and steering controllers have been provided. The thrust has been designed using feedback linearization in order to force convergence of the forward speed to a prespecified value of u_0 . The steering controller is physically realized by a force applied at the rear of the vehicle. This force induces a torque that controls the vehicle's yawing movement and, in doing so, it produces residual sideslip. For parallel formations, we see that the forward speed converges to the desired speed, and the crab angle converges to zero. For circular formations, the crab angle converges to a constant.

When a steady, uniform flow is considered, the forward speed and crab angle of vehicles under parallel formation control also converge as desired. For circular motion, the crab angle is a function of the vehicle's heading; therefore, the rigid body model has been modified so that the steering force is replaced by a moment couple. Additionally, the backstepping control has been replaced with a proportional-integral controller. The proposed controllers are observed to yield the desired formations in simulation.

Ongoing work includes extending the planar rigid-body model to a 3-D model and verifying the results on a multi-vehicle testbed.

Appendix A

Appendix: Alternate Drag Model

Throughout this thesis, the drag force was considered to act through the vehicle's center of mass. In this section the more realistic assumption is used that the drag force acts through the center of pressure a distance l_1 (positive or negative) away from the center of gravity. We denote the moment arm length of the steering force as l_2 . Of the equations of motion derived earlier, only the moment equation changes. The new moment equation becomes

$$\begin{aligned}
 M_k &= (-l_2 \bar{x}_k) \times (F_k \bar{y}_k) + (l_1 \bar{x}_k) \times (-D_k \tilde{x}_k) \\
 &= -l_2 F_k \bar{z}_k - l_1 D_k \sin \beta_k \bar{z}_k \\
 &= (-l_2 F_k - l_1 D_k \sin \beta_k) \bar{z}_k.
 \end{aligned} \tag{A.1}$$

Thus,

$$I_0 \dot{\omega}_k = -l_2 F_k - l_1 D_k \sin \beta_k. \tag{A.2}$$

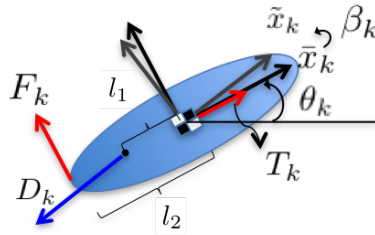


Figure A.1: A rigid-body in a uniform flowfield. The drag is assumed to act a distance l_1 from the center of mass.

Solving for $\dot{\omega}_k$ gives

$$\dot{\omega}_k = -\frac{l_2}{I_0}F_k - \frac{l_1}{I_0}D_k \sin \beta_k, \quad (\text{A.3})$$

where the first term represents the original backstepping controller and the second term is the non-trivial moment due to the relocated drag.

Cancellation of Drag Moment Using Integrator Backstepping

In our previous work (with particles rather than rigid bodies), the backstepping procedure was directed at the rotational dynamics of 6.15. We only sought to regulate the heading and its derivatives (θ_k , $\dot{\theta}_k$, and $\ddot{\theta}_k$). Considering only the velocity and turning rate of each particle, the particle system was

$$\begin{aligned} \dot{\eta}_k &= h(\eta_k) + g(\eta_k)\xi_k \\ \dot{\xi}_k &= a_k, \end{aligned} \quad (\text{A.4})$$

where

$$h(\eta_k) = \begin{bmatrix} \cos \eta_{3,k} \\ \sin \eta_{3,k} \\ 0 \end{bmatrix} \quad \text{and} \quad g(\eta_k) = \begin{bmatrix} 0 \\ 0 \\ 1 \end{bmatrix}.$$

We let $\phi_k(\eta)$ be the desired control of the η dynamics, where $\eta = [\eta_1, \dots, \eta_N]^T$, and using the transformation $z_k = \xi_k - \phi_k(\eta)$, we wrote (A.4) as [16]

$$\begin{aligned} \dot{\eta}_k &= [h(\eta_k) + g(\eta_k)\phi_k(\eta)] + g(\eta_k)z_k \\ \dot{z}_k &= \nu_k, \end{aligned} \quad (\text{A.5})$$

where $a_k = \nu_k + \dot{\phi}_k$ is the backstepping control. Using this procedure, the controllers

that we developed for $\ddot{\theta}_k$ have been used, without alteration, in our rigid body equations of motion; that is, we effectively have $\dot{\omega}_k = a_k$.

When a moment due to the flowfield is present, we extend the system (A.4) to the general case of [16]

$$\begin{aligned}\dot{\eta}_k &= h(\eta_k) + g(\eta_k)\xi_k \\ \dot{\xi}_k &= h'(\eta_k, \xi) + g'(\eta_k, \xi)a_k.\end{aligned}\tag{A.6}$$

Here, $h(\eta_k)$ and $g(\eta_k)$ are as described previously. The equation $\dot{\xi}_k$ represents the angular acceleration. Therefore, $g'(\eta_k) = 1$, a_k represents the desired backstepping controller, and $h'(\eta_k)$ represents the moment due to drag.

As with the particle model, we add and subtract $g(\eta_k)\phi_k(\eta)$ to the right side of the first equation of (A.6) to obtain [16]

$$\begin{aligned}\dot{\eta}_k &= [h(\eta_k) + g(\eta_k)\phi_k(\eta)] + g(\eta_k)[\xi_k - \phi_k(\eta)] \\ \dot{\xi}_k &= h'(\eta_k, \xi) + g'(\eta_k, \xi)a_k.\end{aligned}\tag{A.7}$$

Using the change of variables $z_k = \xi_k - \phi_k(\eta)$ gives [16]

$$\begin{aligned}\dot{\eta}_k &= [h(\eta_k) + g(\eta_k)\phi_k(\eta)] + g(\eta_k)z_k \\ \dot{z}_k &= h'(\eta, \xi) + g'(\eta_k, \xi)a_k - \dot{\phi}_k.\end{aligned}\tag{A.8}$$

We use the transformation $\nu_k = g'(\eta_k, \xi)a_k - \dot{\phi}_k$, which gives us the final form

$$\dot{\eta}_k = [h(\eta_k) + g(\eta_k)\phi_k(\eta)] + g(\eta_k)z_k \quad (\text{A.9})$$

$$\dot{z}_k = \nu_k + h'(\eta, \xi),$$

where $h'(\eta, \xi)$ is the term for the angular acceleration due to drag. To show the stability of the transformed system and determine the backstepping controller a_k , the following composite Lyapunov function is used:

$$V_c = V + \frac{1}{2}z_k^2. \quad (\text{A.10})$$

Taking the time-derivative of (A.10) yields

$$\dot{V}_c = \dot{V} + z_k\dot{z}_k = \dot{V} + z_k(\nu_k + h'(\eta_k, \xi_k)). \quad (\text{A.11})$$

The virtual control ν_k is then chosen to make $\dot{V}_c \leq 0$. This process includes canceling $h'(\eta_k, \xi_k)$, the angular accerelation due to the drag. Below, this procedure is shown for the case of parallel formations, and can be easily extended to the other cases.

Example of Moment Cancellation Using Parallel Formations

Here an example is given of drag moment cancellation using parallel formations (no flow). Recall that the equations of motion for the k th vehicle in a formation are

given by

$$\begin{aligned}
\dot{r}_k &= u_k \bar{x}_k + v_k \bar{y}_k = s_k \tilde{x}_k \\
\dot{u}_k &= -\frac{1}{m_0} D_k \cos \beta_k + \frac{1}{m_0} T_k + v_k \omega_k \\
\dot{v}_k &= -\frac{1}{m_0} D_k \sin \beta_k + \frac{1}{m_0} F_k - u_k \omega_k \\
\dot{\omega}_k &= a_k,
\end{aligned} \tag{A.12}$$

where $\omega_k = \dot{\theta}_k$, $D_k = \frac{1}{2} \rho s_k^2 S C_D$, and $\beta_k = \arctan(v_k/u_k)$. When a moment due to the drag is included, this model becomes

$$\begin{aligned}
\dot{r}_k &= u_k \bar{x}_k + v_k \bar{y}_k = s_k \tilde{x}_k \\
\dot{u}_k &= -\frac{1}{m_0} D_k \cos \beta_k + \frac{1}{m_0} T_k + v_k \omega_k \\
\dot{v}_k &= -\frac{1}{m_0} D_k \sin \beta_k + \frac{1}{m_0} F_k - u_k \omega_k \\
\dot{\omega}_k &= a_k + h',
\end{aligned} \tag{A.13}$$

where $h' = -\frac{l_1}{I_0} D_k \sin \beta_k$. We would like to design a_k using backstepping to drive a collection of vehicles in a parallel formation. Therefore, for ease of control design we follow the backstepping method used for the particle model and consider only the rotational dynamics, given by

$$\dot{\omega}_k = a_k + h'. \tag{A.14}$$

This can be substituted into the angular acceleration equation of model (1.7) to

give:

$$\begin{aligned}
\dot{\eta}_{1,k} &= \cos \eta_k + \langle f_k, 1 \rangle \\
\dot{\eta}_{2,k} &= \sin \eta_k + \langle f_k, i \rangle \\
\dot{\eta}_{3,k} &= \omega_k \\
\dot{\omega}_k &= a_k + h',
\end{aligned} \tag{A.15}$$

where $\eta_k = \theta_k$ is the k th vehicle's heading and $\eta_{n,k}$, $n = 1, \dots, 3$ are the position ($\eta_{1,k}$ and $\eta_{2,k}$) and orientation ($\eta_{3,k}$) of the k th vehicle. To find a suitable controller a_k that takes into account the acceleration due to the drag h' , we begin by defining the Lyapunov function

$$V_{1,c}(\eta, z) = -V_1(\eta) + \frac{1}{2} \sum_{k=1}^N z_k^2, \tag{A.16}$$

where $V_1(\eta) = \frac{1}{2}|p_\theta|^2$. Following the procedure outlined in Section 3.1, we take the derivative of (A.16) as

$$\dot{V}_c = -\frac{1}{N} \sum_{k=1}^N \langle p_\theta, i e^{i\eta_{3,k}} \rangle \dot{\eta}_{3,k} + \sum_{k=1}^N z_k \dot{z}_k. \tag{A.17}$$

Using the transformation $\dot{\eta}_{3,k} = \dot{\phi}_k + \dot{z}_k$ and $\dot{z}_k = \nu_k + h'$ yields

$$\dot{V}_c = \sum_{k=1}^N \left[-\frac{1}{N} \langle p_\theta, i e^{i\eta_{3,k}} \rangle \dot{\phi}_k - \frac{1}{N} \langle p_\theta, i e^{i\eta_{3,k}} \rangle z_k + z_k (\nu_k + h') \right]. \tag{A.18}$$

Choosing $\nu_k = -\kappa z_k - h' + \frac{1}{N} \langle p_\theta, i e^{i\eta_{3,k}} \rangle$ yields

$$\dot{V}_c = \sum_{k=1}^N \left[\frac{K}{N} \langle p_\theta, i e^{i\eta_{3,k}} \rangle^2 - \kappa z_k^2 \right]. \tag{A.19}$$

With ν_k now defined, the backstepping control, given by $a_k = \nu_k + \dot{\phi}_k$, is:

$$a_k = -\kappa z_k - h' + \frac{1}{N} \langle p_\theta, i e^{i\eta_{3,k}} \rangle - \frac{K}{N} \sum_{j=1}^N [\langle e^{i\eta_{3,j}}, e^{i\eta_{3,k}} \rangle (\omega_j - \omega_k)], \quad K < 0. \quad (\text{A.20})$$

When a_k is plugged into $\dot{\omega}_k = a_k + h'$, the system (A.15) becomes

$$\begin{aligned} \dot{\eta}_{1,k} &= \cos \eta_k + \langle f_k, 1 \rangle \\ \dot{\eta}_{2,k} &= \sin \eta_k + \langle f_k, i \rangle \\ \dot{\eta}_{3,k} &= \omega_k \\ \dot{\omega}_k &= a_k, \end{aligned} \quad (\text{A.21})$$

so that now the vehicle using steering controller (A.20) has the same dynamics as a vehicle whose center of pressure is located at its center of mass.

Bibliography

- [1] I. Ali, G. Radice, and J. Kim. Backstepping control design with actuator torque bound for spacecraft attitude maneuver. *Journal of Guidance, Control, and Dynamics*, 33(1):254–259, January-February 2010.
- [2] K. H. Ang, G. Chong, and Y. Li. PID control system analysis, design, and technology. *IEEE Transactions on Control Systems Technology*, 13(4):559–576, July 2005.
- [3] E. Borhaug, A. Pavlov, E. Panteley, and K. Y. Pettersen. Straight line path following for formations of underactuated marine surface vessels. *IEEE Transactions on Control Systems Technology*, 19(3):493 – 506, May 2011.
- [4] E. Borhaug, A. Pavlov, and K. Y. Pettersen. Integral LOS control for path following of underactuated marine surface vessels in the presence of constant ocean currents. In *Proceedings of the 47th IEEE Conference on Decision and Control*, pages 4984 – 4991, Cancun, Mexico, December 2008.
- [5] N. Ceccarelli, M. Di Marco, A. Garulli, and A. Giannitrapani. Collective circular motion of multi-vehicle systems with sensory limitations. In *Proceedings of the 44th IEEE Conference on Decision and Control, and the European Control Conference 2005*, pages 740–745, Seville, Spain, December 2005.
- [6] Y. Y. Chen and Y. Tian. A backstepping design for directed formation control of three-coleader agents in the plane. *International Journal of Robust and Nonlinear Control*, 19(7):729–745, 2008.
- [7] D. Crimmins and J. Manley. Remus AUV. {<http://oceanexplorer.noaa.gov/explorations/08auvfest/background/auvs/auvs.html>}, August 2010. Last Checked: 07-11-2011.
- [8] P. Ferguson and J. How. Decentralized estimation algorithms for formation flying spacecraft. In *AIAA Guidance, Navigation, and Control Conference and Exhibit*, Austin, Texas, August 2003.
- [9] R. Fierro and F. L. Lewis. Control of a nonholonomic mobile robot: Backstepping kinematics into dynamics. In *Proceedings of the 34th IEEE Conference on Decision and Control*, pages 3805–3810, New Orleans, LA, December 1995.
- [10] E. Frazzoli, M. A. Dahleh, and E. Feron. Real-time motion planning for agile autonomous vehicles. *Journal of Guidance, Control, and Dynamics*, 25(1):116–129, January - February 2002.
- [11] E. W. Frew, D. A. Lawrence, and S. Morris. Coordinated standoff tracking of moving targets using Lyapunov guidance vector fields. *J. Guidance, Control, and Dynamics*, 31(2):290–306, 2008.

- [12] J. A. Gallian. *Contemporary Abstract Algebra*. R. Stratton, Brooks/Cole, 10 Davis Drive, Belmont, CA 94002-3098 USA, 7th edition, 2006.
- [13] M. Hutagalung, T. Hayakawa, and T. Urakubo. Configuration consensus of two underactuated planar rigid bodies. pages 5016 – 5021, Cancun, Mexico, December 2008. 47th IEEE Conference on Decision and Control.
- [14] Z. Jiang and H. Nijmeijer. Tracking control of mobile robots: A case study in backstepping. *Automatica*, 33(7):1393 – 1399, 1997.
- [15] E. W. Justh and P. S. Krishnaprasad. Equilibria and steering laws for planar formations. *Systems and Control Letters*, 52(1):25–38, May 2004.
- [16] H. Khalil. *Nonlinear Systems*. Prentice Hall, Upper Saddle River, NJ 07458, 3rd. edition, 2002.
- [17] P. Kokotovic and M. Arcak. Constructive nonlinear control: a historical perspective. *Automatica*, 37(5):637–662, 2001.
- [18] K. D. Listmann and C. A. Woolsey. Output synchronization of systems in chained form. In *Joint 48th IEEE Conference on Decision and Control and 28th Chinese Control Conference*, pages 3341 – 3346, Shanghai, P.R. China, December 2009.
- [19] R. Mahoney and T. Hamel. Stable tracking control for unmanned aerial vehicles using non-inertial measurements. Proceedings of the 39th IEEE Conference on Decision and Control, pages 2971 – 2976, Sydney, Australia, December 2000.
- [20] A. Makarenko and H. F. Durrant-Whyte. Decentralized data fusion and control in active sensor networks. In *International Conference on Information Fusion*, Stockholm, Sweden, 2004.
- [21] J. A. Marshall, M. E. Broucke, and B. A. Francis. Formations of vehicles in cyclic pursuit. *IEEE Trans. Automatic Control*, 49(11):1963–1974, 2004.
- [22] R. Mellish, S. Naporá, and D. A. Paley. Backstepping control design for motion coordination of self-propelled vehicles in a flowfield. *International Journal of Robust and Nonlinear Control*, 21(12):1452–1466, August 2011.
- [23] F. Mirzaei, A. Mourikis, and S. Roumeliotis. “Performance Characterization of Cooperative Localization and Tracking.” {<http://mars.cs.umn.edu/projects/-current/PerformanceCLATT/PerformanceCLATT.html>}. Last Checked: 08-06-2011.
- [24] N. Moshtagh and A. Jadbabaie. Steering laws for distributed motion coordination of kinematic agents in three dimensions. 47th IEEE Conference on Decision and Control, pages 1741–1746, Cancun, Mexico, December 2008.

- [25] R. M. Murray, Z. Li, and S. S. Sastry. *A Mathematical Introduction to Robotic Manipulation*. CRC Press, Taylor and Francis Group, 6000 Broken Sound Parkway NW, Suite 300, Boca Raton, FL 33487-2742, 1994.
- [26] S. Napora and D. A. Paley. Observer-based feedback control for stabilization of collective motion. To appear in *IEEE Transactions on Automatic Control*.
- [27] D. A. Paley and C. Peterson. Stabilization of collective motion in a time-invariant flowfield. *Journal of Guidance, Control, and Dynamics*, 32(3):771–779, May–June 2009.
- [28] D. A. Paley and D. Warshawsky. Reduced-order dynamic modeling and stabilizing control of a micro-helicopter. In *Proceedings of the 47th AIAA Aerospace Sciences Meeting including the New Horizons Forum and Aerospace Exposition*, Orlando, Florida, January 2009.
- [29] C. Peterson and D. A. Paley. Multi-vehicle coordination in an estimated time-varying flowfield. *AIAA Journal of Guidance, Control, and Dynamics*, 34(1):177–191, 2011.
- [30] C. W. Reynolds. Flocks, herds, and schools: A distributed behavioral model. In *Computer Graphics*, volume 21 of *SIGGRAPH '87 Conference Proceedings*, pages 25–34, 1987.
- [31] J. Roberts, M. Dunbabin, A. Tews, W. Hu, and R. Zlot. “Multirobot Cooperation.” {<http://research.ict.csiro.au/research/labs/autonomous-systems/sensor-networks/robot-sensor-network-interaction>}, May 2010. Last Checked: 08-05-2011.
- [32] R. Sepulchre, M. Jankovic, and P. V. Kokotovic. *Constructive Nonlinear Control*. Springer, New York, 1997.
- [33] R. Sepulchre, D. A. Paley, and N. E. Leonard. Stabilization of planar collective motion: All-to-all communication. *IEEE Transactions on Automatic Control*, 52(5):811–824, May 2007.
- [34] R. Sepulchre, D. A. Paley, and N. E. Leonard. Stabilization of planar collective motion with limited communication. *IEEE Transactions on Automatic Control*, 53(3):706–719, April 2008.
- [35] L. Techy, D. A. Paley, and C. A. Woolsey. UAV coordination on convex curves in wind: An environmental sampling application. 2009 European Control Conference, pages 4967–4972, Budapest, Hungary, August 2009.
- [36] F. Zhang, M. Goldgeier, and P. S. Krishnaprasad. Control of small formations using shape coordinates. volume 2, pages 2510–2515, Taipei, Taiwan, September 2003. International Conference on Robotics and Automation.